The EBEX Cryostat and Supporting Electronics

A DISSERTATION
SUBMITTED TO THE FACULTY OF THE GRADUATE SCHOOL
OF THE UNIVERSITY OF MINNESOTA
BY

Ilan Shai Sagiv

IN PARTIAL FULFILLMENT OF THE REQUIREMENTS
FOR THE DEGREE OF
Doctor of Philosophy

Professor Shaul Hanany

April, 2011

Acknowledgements

First and foremost, I would like to thank my advisor, Shaul Hanany, for his support and guidance. Shaul has taught me that success in experimental physics lies in the small details; I am fortunate to have learned from his uncompromising professionalism.

Special thanks go to Loren Levinson and his Electronics and Data Acquisition Group at the Weizmann Institute of Science. Loren, I appreciate your advice and help.

Working on EBEX has been a greatly rewarding experience. My deepest thanks go to the entire collaboration. The sense of camaraderie that we built made us so much more than just a scientific collaboration.

I especially want to highlight my Cosmo-lab mates and EBEX experimental team: Asad Aboobaker, Franǫis Aubin, Chaoyun Bao, Daniel Chapman, Joy Didier, Matt Dobbs, Will Grainger, Seth Hillbrand, Hannes Hubmayr, Jeff Klein, Michele Limon, Kevin MacDermid, Amber Miller, Michael Milligan, Dan Polsgrove, Kate Raach, Britt Reichborn-Kjennerud, Greg Tucker, Jerry Vinokurov and Kyle Zilic. You guys made working on EBEX in the lab, at Nevis and in New Mexico a memorable experience.

To the University of Minnesota Physics & Astronomy machine shop: you were an endless source of good suggestions. Your willingness to help goes far beyond the call of duty.

On a personal level, I thank my parents, Linda and Menachem Sagiv. Thank you for your love and encouragement throughout the years. My curiosity about the universe was sparked by our Friday afternoon family ritual of watching Carl Sagan's Cosmos together when I was a child.

To my children, Zohar and Gilad, I know you believe that bubble wrap is the most fascinating thing in my lab. Maybe one day I can convince you otherwise. Thank you for being my utmost joy.

And finally, to Yasmin, my wife, I can not emphasize your contribution enough. Your encouragement and love helped me through the toughest times. I am grateful for your willingness to join me in bearing the long Minnesotan winters. Your positivity and strength are my inspiration. Thank you.

Abstract

EBEX is a balloon-borne polarimeter designed to measure the B-mode polarization of the cosmic microwave background radiation. The instrument includes a 1.5 meter Gregorian-type telescope and a cryogenic receiver housing 1432 bolometric transition edge sensor detectors operating at 0.3° K. In this thesis I describe my work on the development and characterization of the EBEX cryogenic system and of several electronics sub-systems.

I developed CANbus-based software to monitor temperatures inside the receiver and to control the operation of two sub-Kelvin adsorption refrigerators. I commissioned and tested an experiment-wide timing system that tags data from all subsystems with an accuracy that is a factor of 10 better than required. I constructed and tested two pressure vessels that store data on board.

Data collected during the EBEX test flight in June 2009 show that all these subsystems performed according to predictions. The temperatures of the cryostat were stable. An analysis of the temperature data finds no scan synchronous signal in the cryostat temperatures. The timing system and pressure vessels operated as expected.

A calibrator was installed inside the receiver to monitor detector responsivity variations. I analyzed the data from the test flight and show that in its current configuration the calibrator is inadequate.

Contents

List of Tables

List of Figures

Chapter 1

Introduction

Many theories have appeared and faded over the past millennia for describing how the universe began, ranging from a universe that rests on a stack of turtles [1] to a static steady-state universe obeying Einstein's equations. The model that has survived all the observational evidence is that of a universe that began in a very hot and dense state and has been cooling since by expansion.

The strongest evidence for this model is the presence of a cosmic microwave background (CMB) [2] resulting from the decoupling of photons from plasma when protons, helium nuclei and electrons combined into neutral hydrogen and helium. The photons were left to stream freely through the universe, carrying with them information about the early stages of the evolution of the universe.

This thesis focuses on EBEX, a balloon-borne experiment designed to measure the polarization of the CMB.

1.1 Inflation and The Standard Cosmological Model

In the last two decades, technological advancement has made possible the measurement of cosmological parameters with an accuracy of a few percent [3]. The picture that unambiguously arises from these measurements is that of a spatially flat universe that is dominated by cold dark matter and a cosmological constant, in which the universe underwent exponential inflation within its first few fractions of a second [4].

However, there is a wide range of theories that describe this inflation and a variety

of open questions regarding its mechanism and parameters [5].

1.2 CMB Temperature Anisotropies

The blackbody temperature of the CMB is highly uniform across the sky with primordial anisotropy appearing at the level of 1 part in 10^5 [6][7]. According to the standard cosmological model these anisotropies are due to quantum fluctuations in the primordial environment that were inflated to macroscopic spacial density variations.

For analysis purposes, it is useful to decompose the temperature as a function of position on the sky $\hat{n}$ into spherical harmonics $Y_{\ell m}$:

$$T(\hat{n}) = \sum_{\ell,m} a_{\ell m} Y_{\ell m}(\hat{n}) \tag{1.1}$$

The power in each mode ℓ is then given by the variance of the $a_{\ell m}$:

$$C_\ell = < |a_{\ell m}|^2 > = \frac{1}{2\ell + 1} \sum_m |a_{\ell m}|^2 \tag{1.2}$$

Figure 1.1 shows the temperature power spectrum from the latest 7-year results from the Wilkinson Microwave Anisotropy Probe (WMAP) [8].

1.3 CMB Polarization

The CMB is linearly polarized due to Thomson scattering just before recombination [9]. In order to produce a net polarization, the photon field must include a quadropole anisotropy. The polarization field can be decomposed into a curl-free E-mode polarization and a gradient-free B-mode polarization.[1] The different polarization patterns are created by different physical mechanisms. The E-modes are created by density perturbations, which are scalar perturbations in the space-time metric. The B-modes are created by tensor perturbations of the metric which are gravity waves [10]. Inflation models predict a stochastic background of gravity waves. The amplitude of the gravity waves is proportional to the energy scale of inflation. The presence of these gravity waves during recombination will produce B-mode[2] polarization in the CMB.

[1] The names E and B come from an analogy to electromagnetism

[2] as well as E-modes

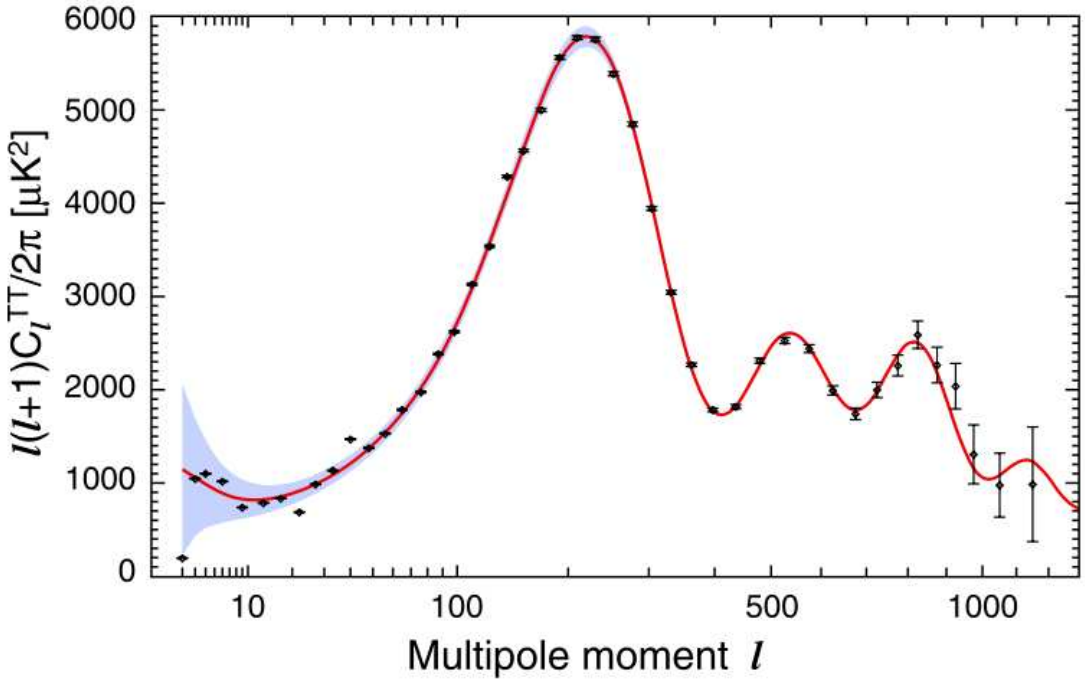

Figure 1.1: Temperature power spectrum of the CMB from WMAP 7 year results [8]. The red line is the best fit cosmological model.

Therefore, a detection of B-modes will be a direct probe of this energy scale. Different inflationary models predict a different ratio between the tensor and scalar contributions to the CMB quadropole perturbations, denoted by r. The amplitudes of the B-mode signal is proportional to this ratio. A detection of primordial B-modes in the CMB will be an unambiguous signature of inflation and will help constrain the parameters which describe it.

1.4 Current Status

The B-mode signal is extremely faint with the peak of the power spectrum at <150°nK. The current upper limit on the tensor-to-scalar ratio is $r = 0.24$ [3]. Radiation originating in our galaxy may obscure the B-mode signal. In particular, synchrotron and dust emission are the dominant foregrounds in the relevant frequencies [12]. There are

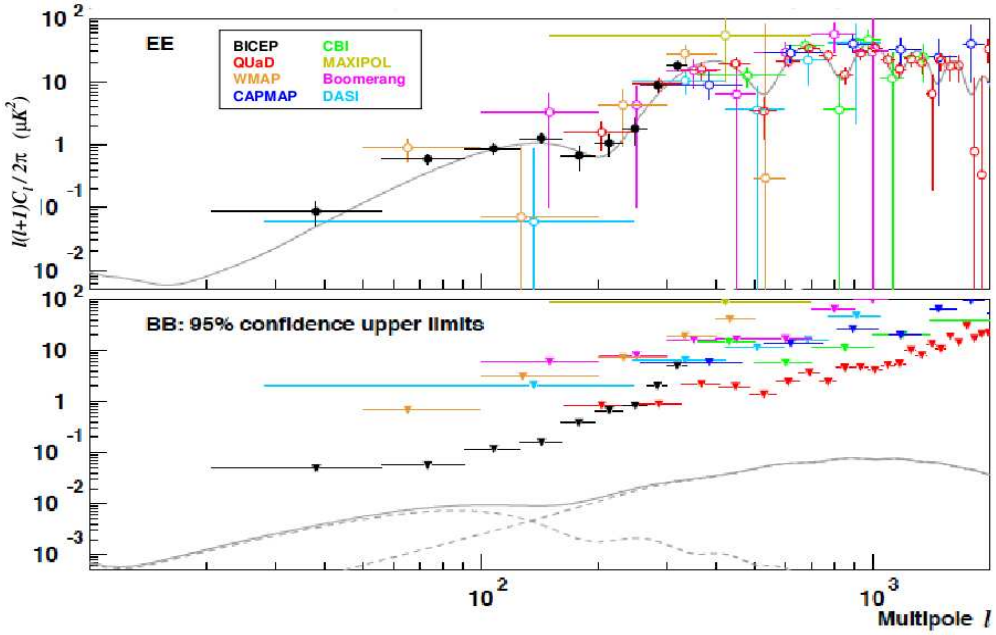

Figure 1.2: E and B power spectra compilation of existing data from CMB polarization experiments. Theoretical spectra from a ΛCDM model with r = 0.1 are shown for comparison; the BB curve is the sum of the inflationary and gravitational lensing components. Plot from [11]

uncertainties about the level of the polarized galactic dust at the accuracies required for a B-mode signal detection. Nevertheless, any measurement of the B-mode signal would require characterization and removal of the dust foreground [13].

In addition, the CMB photons are gravitationally lensed by intervening large scale structure in the universe. Lensing of the CMB distorts the anisotropy pattern on the sky, modifies its power spectrum [14], and creates B-mode polarization even in the absence of gravity waves [15].

The CMB has been measured by a host of ground-based and balloon-borne experiments, and by three satellites missions (COBE, WMAP and PLANCK). The temperature and spectrum of the CMB have been well characterized. E mode polarization has been detected by several experiments and mapped between $40 < \ell < 1300$. Figure 1.2 shows recent measurements of the E and B-mode power spectra. Neither the

gravitational wave nor the lensing B-mode signal have been detected.

1.5 Thesis Overview

This thesis focuses on EBEX, a balloon-borne experiment designed to measure the polarization of the CMB at high sensitivity. EBEX is a complex experiment. It includes several subsystems not all described in detail in this thesis. Here I focus on my contribution to EBEX specifically in development and characterization of the cryogenics system and its supporting electronics. Chapter 2 gives a general overview of the EBEX experiment and its science goals. Chapter 3 describes the EBEX timing system. Chapter 4 reviews the novel electronics boards developed for monitoring the cryostat housekeeping. Chapter 5 describes the hard drive pressure vessel. Chapter 6 reviews the power system and grounding design. Chapter 7 gives a review of the calibrator flashes used during the test flight and an analysis of their performance.

Chapter 2

The EBEX Instrument

EBEX (E and B EXperiment) is a balloon-borne experiment that is designed to measure the polarization and temperature of the Cosmic Microwave Background (CMB) at an angular resolution corresponding to $20 < \ell < 1500$. EBEX completed a 14 hour test flight from Fort Sumner, New Mexico in June 2009. The experiment is in preparation for a 14-day long duration ballooning (LDB) science flight above Antarctica in December 2011.

2.1 Science Goals

EBEX has several goals. The first is to search for the B-mode polarization of the CMB. Figure 2.1 shows the expected power spectrum of both E and B modes for $\ell < 1200$, assuming the tensor to scalar ratio is 0.1. If this assumption is accurate EBEX will have the sensitivity to detect the inflationary B-mode signal. Otherwise, EBEX will set an upper limit of $r < 0.04$, a significant improvement on current measurements.

The second goal is to characterize Galactic polarized dust emission and to determine its angular power spectra in both E and B-mode polarizations at the micro-Kelvin level. Characterization of dust foregrounds is a key element in extracting the B-mode signal [16],[17].

The third goal is to measure the predicted but yet undetected lensing of the CMB. Gravitational lensing of the CMB distorts the anisotropy pattern on the sky, modifies its power spectrum [14], and converts E-mode to B-mode polarization [15].

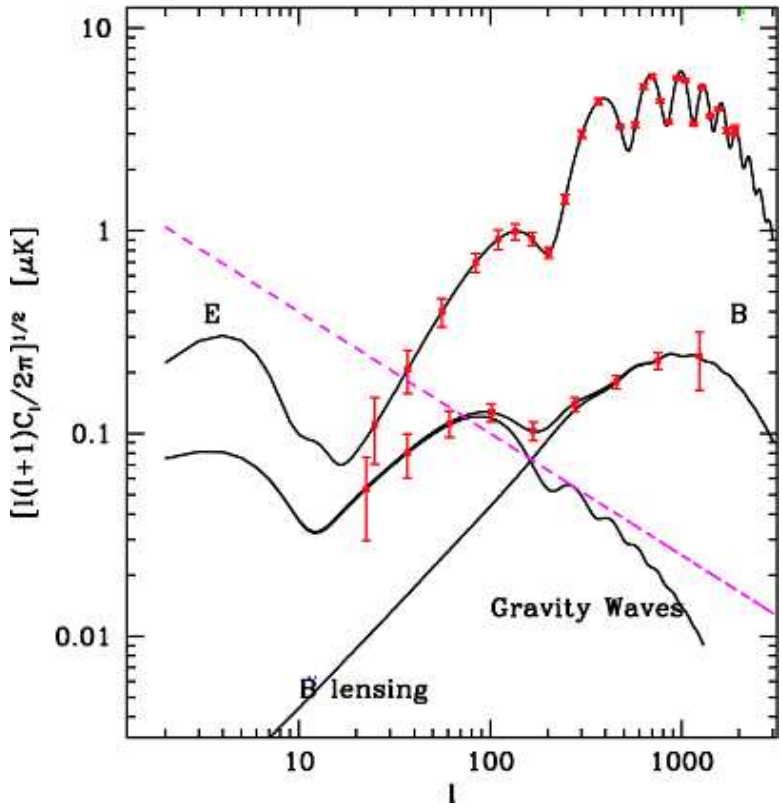

Figure 2.1: Solid black lines are theoretical E- and B-mode power spectra, identical to those shown in figure 1.2. Red data points represent expected EBEX results (with 1σ error bars) assuming a 14-day flight. The dashed pink line is the expected dust BB spectra at the 150 GHz band, assuming the LDB scan region, extrapolated from WMAP observations.

2.2 Instrument Overview

The EBEX instrument, shown in figure 2.2 is a microwave telescope with an 8 arc-minute beam measuring at three frequency bands. The required sensitivity is achieved by using many bolometric detectors with a long integration time. Polarization is measured using a rotating half-wave plate (HWP) and fixed wire grid.

The instrument hangs from a helium balloon floating at an altitude of ∼40 km where

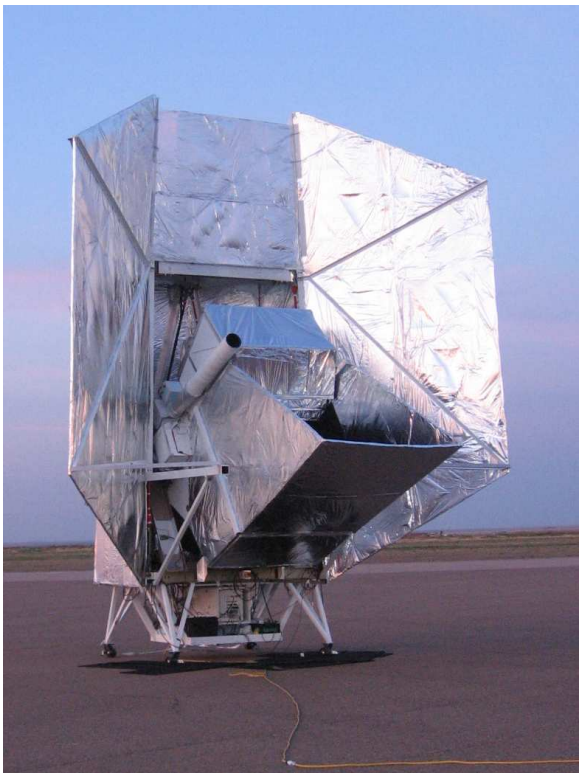

Figure 2.2: The EBEX payload on the ground with baffles during ground tests.

atmospheric emission is more than two orders of magnitude lower than at sea level. In addition, measuring from balloon altitudes enables measuring at frequencies that are absorbed by the atmosphere. EBEX will scan $\sim 1\%$ of the sky at high galactic latitudes where galactic dust emission is low. Each pixel in the observed patch will be revisited over 10^7 times.

EBEX has three frequency bands covering the range between 130 GHz and 450 GHz. The wide frequency range provides a strong lever arm for estimating the galactic dust foreground. Galactic dust emission is dominant at high frequency bands where it will be measured, interpolated and subtracted from the lower frequency bands, where the CMB is dominant.

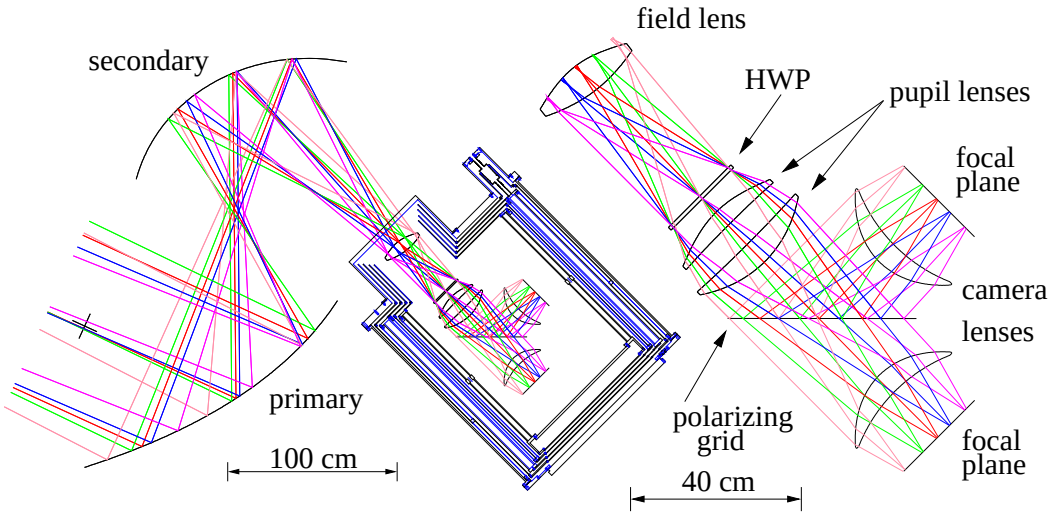

Figure 2.3: Left: Two mirrors focus light from the sky into the cryostat; Right: The cold optics inside the cryostat.

2.3 Optical Design

EBEX employs a Gregorian-type telescope to focus a microwave beam into a cryostat receiver (figure 2.3). The telescope includes a 1.5 m primary mirror and 1 m ellipsoidal secondary mirror. Inside the cryostat, light passes through several optical elements before arriving at two focal planes populated with bolometric Transition Edge Sensor (TES) detectors [18]. For each detector, regardless of frequency, the beam generated is designed to be a Gaussian with a width of 8 arc-minutes at half the peak value.

2.4 The Attitude Control System

The telescope is mounted on a structure called the gondola which includes a variety of sensors and motors that measure and control its orientation. The pointing of the telescope is controlled by the Attitude Control System (ACS) which is strongly based on experience from the Balloon-borne Large Aperture Sub-millimeter Telescope (BLAST)[19].

A reaction wheel and a pivot motor control the rotation of the gondola. The inner

frame (figure 2.4), which can pivot about an axis, is driven by a linear actuator which controls the elevation angle of the telescope.

The ACS relies on a combination of coarse and fine sensors to point the gondola. Coarse sensors provide an approximate attitude used for real-time pointing. The coarse sensors include a magnetometer, a sun sensor, a differential Global Positioning System (dGPS), an elevation encoder, and a clinometer [20]. The fine sensors include four gyroscopes and two star cameras. The information received from the various sensors is integrated into a feedback loop by the flight computer, which then issues commands to the elevation drive and azimuthal motors.

2.5 The Cryostat

2.5.1 Overall Design

The cryostat [21], shown in a cross-section view in Figure 2.5, holds the cold optics and detectors. It has a diameter of 122 cm and is 150 cm tall, with an optics snout extending an additional 30 cm. The original toroidal liquid helium tank had a capacity of 67 liters that was surrounded by a liquid nitrogen tank containing 120 liters. The cryostat also has two intermediate vapor cooled shields operating at ∼30 K and ∼185 K. During the flight the cryogens are kept at atmospheric pressure by an absolute pressure regulator valve.

The load on the liquid nitrogen is dominated by the conduction and radiation from the warmer outer stages. The load on the liquid helium stage also includes a significant contribution from optical loading from the cryostat's 300°K window.

The cryogen hold-time was measured and found to be significantly lower than expected due to optical loading through the window on the helium stage.

Subsequently, new cryogen tanks were designed and installed in the cryostat after the test flight. The new tanks have a capacity of 130 liters for both nitrogen and helium. With the new tanks the measured hold time has increased to 18 days.

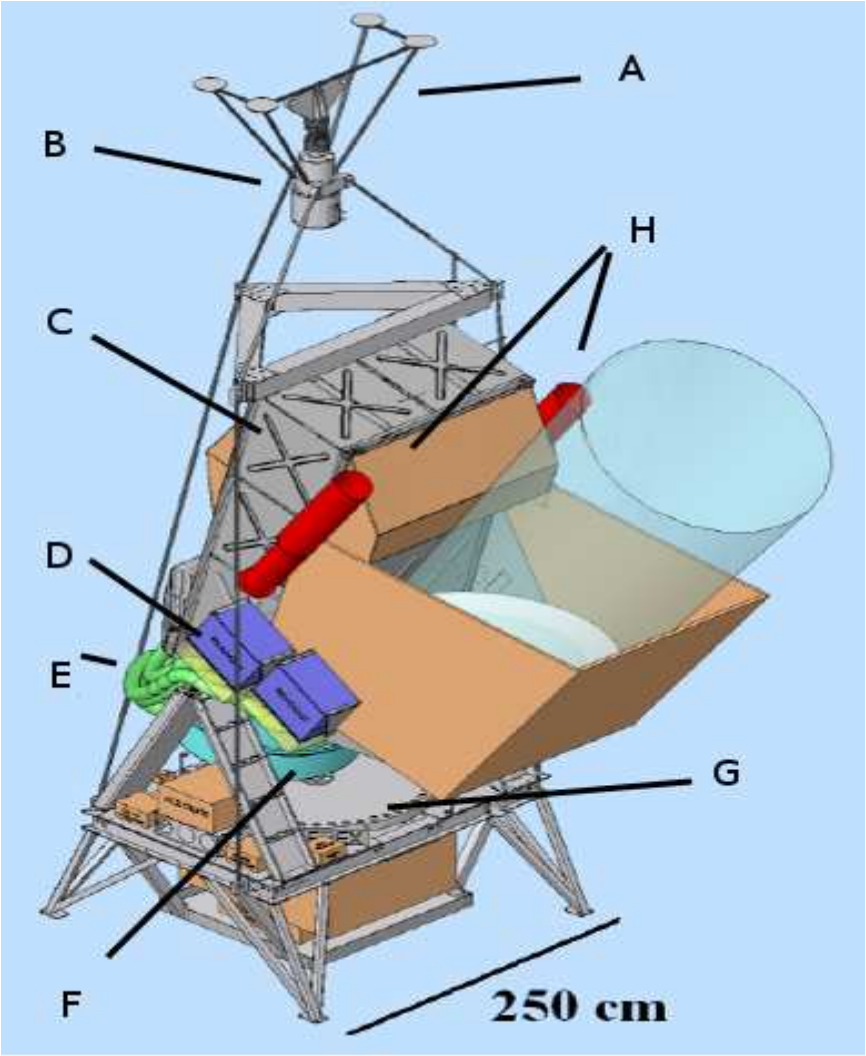

Figure 2.4: A solid model of the EBEX instrument. An inner frame(C) which holds the mirrors and the cryostat (F) pivots about the axis. Azimuthal pointing is accomplished by a combination of reaction wheel (G) and pivot motor (B). A dGPS (A) is used for determination of the pointing in real time (along with other sensors not shown). Two readout crates mounted on each side record the bolometer data (D) (only two crates were used in the test flight). The cables from the cryostat to the readout crate are routed inside a metal bellows tube (E). Two star cameras (H) are used for accurate pointing reconstruction (only one star camera was used in the test flight).

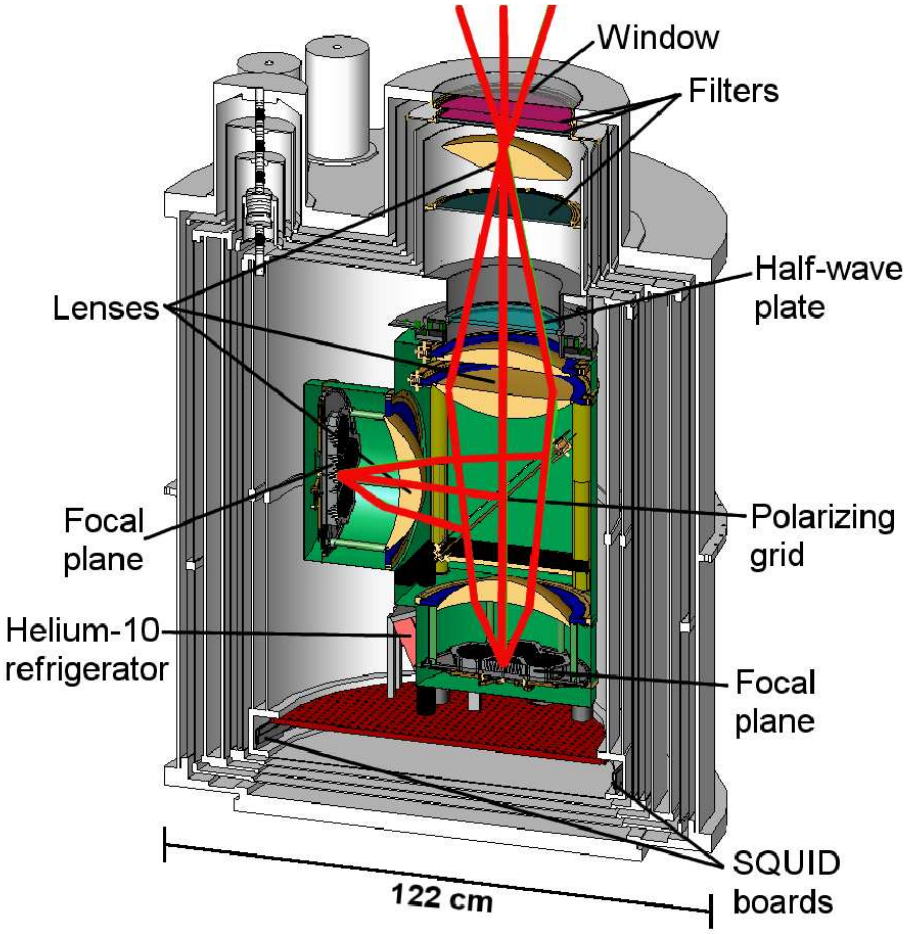

Figure 2.5: A cross section model view of the EBEX cryostat.

2.5.2 Optics

A 12.7 mm thick ultra-high molecular weight polyethylene (UHMWPE) window is mounted at the entrance to the evacuated cryostat. In order to reduce optical loading from this window during the Antarctic flight, it will be removed from the optical path by a motorized mechanism, leaving a 1 mm UHMWPE window. This will happen once the experiment reaches float altitude, where the pressure differential is a few Torr.

A series of filters [22], which were designed and manufactured by colleagues at Cardiff University, are shown in figure 2.6. The filters are designed to prevent high-frequency thermal radiation from reaching the cold optics and the detectors. The cutoff frequencies of the different filters are specified in table 2.1.

Filter Name	Cutoff Freq.
Therm1	60 THz
Therm2	30 THz
Therm3	15 THz
Therm4	12 THz
LPE1	750 GHz
LPE2	600 GHz
LPE2b	540 GHz

Table 2.1: Filters used in EBEX cryostat

Three types of filters are used: 'thermal' filters with low emissivity and high cutoff frequencies, 'Low-Pass Edge' (LPE) filters with lower cutoff frequencies, and a 12.7 mm thick Teflon low-pass filter which has low emissivity in the EBEX bands. The Teflon filter has absorption greater than 90% at frequencies above 10 THz.

An achromatic HWP [23],[24] is mounted on the sky side of a 22 cm diameter aperture stop (Figure 2.6). The HWP is continuously rotated at 2 Hz on a superconducting magnetic bearing (SMB) [25] by a Kevlar belt that is driven by a DC motor mounted outside the cryostat. The angular orientation of the HWP is encoded with a slotted ring illuminated by a laser. The HWP angular orientation can be reconstructed with accuracy better than 0.1° [26].

A 43.5 cm diameter polarizing wire grid is mounted at 45° relative to the incident

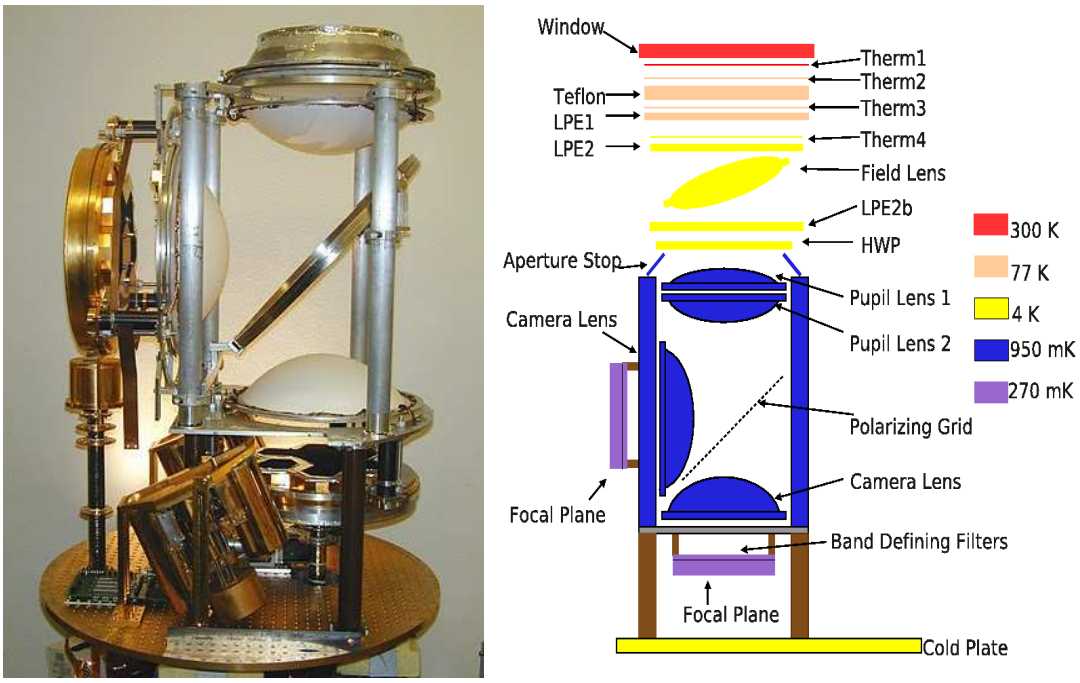

Figure 2.6: EBEX cold optics, color-coded by temperature.

radiation, splitting the beam to the two focal planes. Distributed along the optical path are four lenses per focal plane, all made from a single block of UHMWPE. The lenses provide a flat and telecentric focal plane suitable for the TES arrays. The lenses are coated with a broad-band anti-reflection coating. Light is coupled to the bolometers by a gold-plated array of smooth-walled conical horns and a wave-guide. The wave-guide geometry serves as a high-pass filter and determines the low end cutoff for each of the three bands. A pair of metal-mesh low-pass filters is mounted on the sky side of the horn arrays to define the high end cutoff. These elements define the spectral response of the instrument, spanning 133- 173 GHz (the 150 GHz band), 217-288 GHz (the 250 GHz band) and 355-450 GHz (the 410 GHz band).

2.5.3 Bolometers and readout

Each focal plane includes all three frequency bands with a total of 768, 384, and 280 detectors in each band respectively. The design parameters of the bolometers are optimized for the lower optical loading at balloon altitudes.

Figure 2.7 shows the detector layout for one focal plane. Each focal plane includes seven 8 cm diameter silicon bolometer wafers. Each wafer observes at a single frequency band.

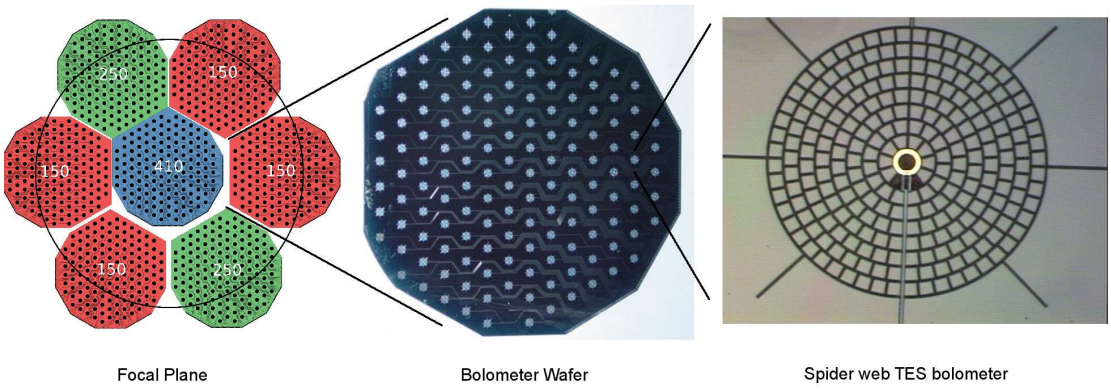

Figure 2.7: Left: A single EBEX focal plane including two 150 GHz wafers, two 250 GHz wafers and a single 410 GHz wafer. Middle: A single bolometer wafer including 144 detectors. Right: A single spider web TES bolometer.

The bolometers are read out using a novel low power digital frequency multiplexing (Dfmux) scheme and series array SQUID amplifiers [27] [28]. Each SQUID reads out 12 bolometers, thus limiting the total number of wires required between the cryogenic stages to 1,110. If the multiplexing factor is increased to 16, the same number of wires will enable reading out a total of 1920 detectors. Efforts are on going to achieve this goal. These wires, which control the SQUIDs and bring the bolometer bias and output signals in and out of the cryostat, are made of manganin weaved into Nomex ribbons [29]. The load on the liquid He stage from these ribbons is 30 mW. In addition, there are another 248 wires used for cryostat housekeeping. The housekeeping wires add another 4.5 mW of load to the liquid helium stage.

2.5.4 Adsorption Refrigerators

The lenses, grid and supporting structure are cooled with a two-stage ^{4}He/^{4}He ('He8') adsorption refrigerator which was measured to maintain a temperature of ∼950 mK with a load of 200 μW for ∼4 days [30]. The bolometers and focal planes are cooled using a three-stage ^{4}He/^{3}He/^{3}He ('He10') adsorption refrigerator which was measured to maintain a temperature of ∼270 mK with a load of 6 μW for ∼5 days. Figure 2.6 shows the cold optics color coded by typical runtime temperature.

Figure 2.8 shows the temperature of the He10 (left) and He8 (right) refrigerators under various loads. The operating load in EBEX is approximately 6μW for the He10 and 200μW for the He8 (right).

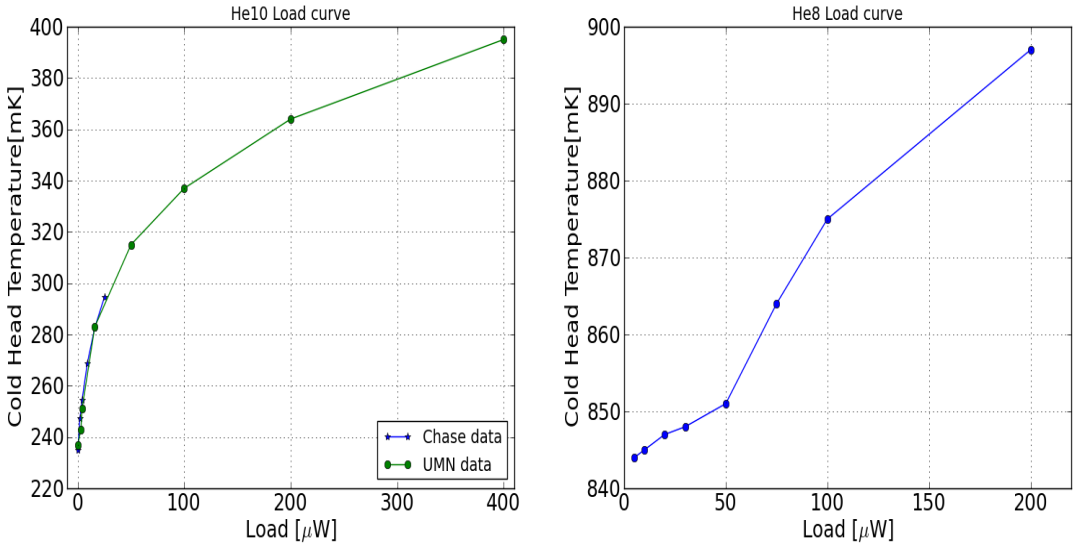

Figure 2.8: Load curve of the He10 refrigerator (right) and of the He8 refrigerator (left).

The refrigerators operate by condensing liquid helium and pumping it back using a charcoal cryopump. To achieve condensation, electrical power is initially applied to a heater element in the cryopump (∼2 W). When the helium is desorbed, the heater is turned off and the gas is cooled and liquefied. Once the helium has condensed, the corresponding gas-gap switch is turned on. This links the cryopump to 4.2°K and

initiates cooling of the refrigerator's cold head. The cold head remains cold until the helium runs out. The He10 (He8) includes three (two) such stages. Both refrigerators are cycled in parallel. Recycling the EBEX adsorption refrigerators consumes approximately 12 liters of liquid helium and lasts around four hours.

2.5.5 RF Mitigation

Radio frequency (RF) interference might be a source of disturbance that couples into the detector signals. Possible sources for RF interference are transmitters on board the gondola as well as motors and other 'noisy' electronics in the instrument. The design for RF mitigation is shown schematically in figure 2.9. The inner volume of the cryostat is not considered RF clean due to the large window. Indium seals and RF gaskets [31] are used to keep all other parts of the cryostat RF clean. To prevent RF interference from entering between the cryostat layers while not compromising the cryogenic performance, 25.4 μm thick stainless steel sheets are wrapped around the optics snout. Wires that penetrate the RF tight area are filtered using capacitive low-pass filters [32],[33]. A high-pass wave guide with a cut-off frequency at 230 GHz is installed on the cold plate (figure 2.6) to allow pumping out of the inner volume. The conical horns, coupling the light to the focal-plane, place the detectors inside a Faraday cage where they are shielded from electromagnetic interference which may enter the cryostat window. A thermally isolating 'RF tower' is created from Vespel wrapped with 5 μm thick superconducting niobium foil. Detector wiring is routed through this tower to keep the wiring in the RF clean area. The detector wiring from the cryostat to the readout crates is wrapped in bronze wool and is routed through a flexible metal hose.

2.6 Test Flight

On June 11, 2009 EBEX was launched on an engineering test flight from NASA's Columbia Scientific Ballooning Facility in Fort Sumner, New Mexico. The experiment remained at an altitude above 35 km for more than 10 hours. EBEX was the first experiment to successfully operate arrays of TES bolometers read out by SQUID amplifiers in a space-like environment. SQUIDs and bolometers were tuned during the flight and maintained their stability. The HWP rotated continuously at 2 Hz throughout the

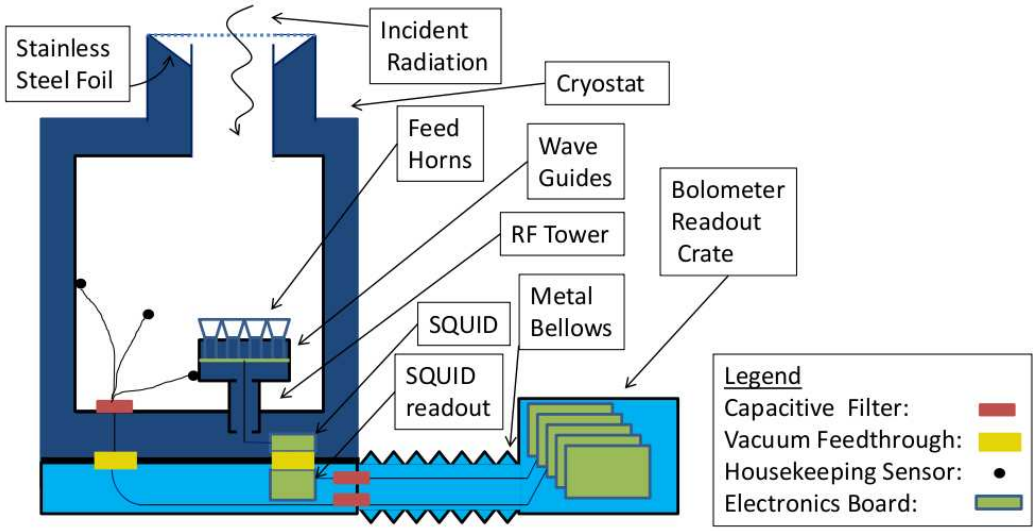

Figure 2.9: Schematic of the EBEX RF mitigation strategy. Blue (Cyan) areas are RF shielded inside (outside) the cryostat.

flight.

There was no evidence of cosmic ray hits in the housekeeping data. The readout boards proved to be robust in a balloon environment.

For the test flight, a stripped down version of the full instrument was used. Only one focal plane with three bolometer wafers was installed. There was one bolometer wafer per frequency band.

The Launch occurred at 14:00 UTC (08:00 local time) and the payload reached floating altitude at 17:00 UTC (11:00 local time). Termination occurred close to 4:00 UTC on June 12 (22:00 local time) as the payload approached California airspace (figure 2.10). During the whole flight, data was transmitted down and commands were sent to the payload via line-of-sight transmitters, first from the main base in Fort Sumner, and later from a down-range station in Winslow, Arizona. Figure 2.10 shows a map with the test flight trajectory.

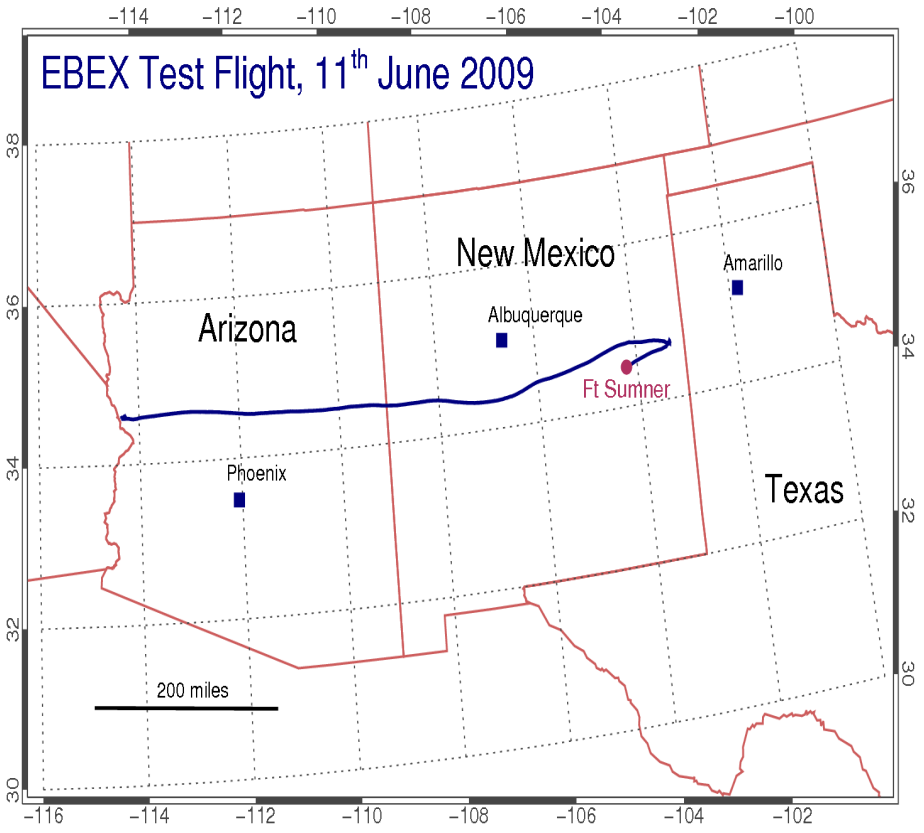

Figure 2.10: The flight trajectory of EBEX during the June 2009 test flight

Chapter 3

Timing

Every data sample in EBEX has a time stamp associated with it. The time stamp is the tick counter of a local clock. The sample rate and time of sampling vary from subsystem to subsystem. Therefore, in order to synchronize the various clocks, a time synchronization system was built. I commissioned and tested the EBEX timing system and assessed its performance during the test flight.

Required Timing Accuracy

Knowing the absolute time of day to within 30 seconds is required for accurate real time pointing at a level of the beam resolution.

To achieve the EBEX science goals (see chapter 1) the pointing of the instrument must be reconstructed for each bolometer data point with an accuracy better than 9 arc-seconds [34]. This comes from requiring that the contamination to the power spectrum from pointing error will be $1/10^{th}$ of the signal.

The bolometer data is recorded at a rate of 190.73 Hz. Pointing sensors are sampled at 5.008 Hz (slow) and 100.16 Hz (fast). Half Wave Plate (HWP) encoders are sampled at 3.05 kHz. Therefore, the data points must be aligned to a single time in a procedure described in section 3.3.4. Errors in the relative timing between subsystems lead to errors in the data alignment. The EBEX timing system is designed to provide relative timing between subsystems that is better than 10 μs.

3.1 EBEX Time Stamp

The EBEX time stamp is a 48-bit long word consisting of a 2-bit Board ID, a 14-bit Major Period register and a 32-bit tick counter (table 3.1). The time stamp is the number of 10 μsec ticks from the start of a six hour Major Period. Each subsystem has a 100 kHz oscillator incrementing the tick counter which is the local copy of the time stamp.

	Source ID	Major Period	Tick counter-High	Tick counter -Low	
# of bits	2	14	18	14	
Time sync	34 bits sent			Set to zero at sync	
CANbus sync	40 bit sent				not sent

Table 3.1: The EBEX time stamp: enumerating from the highest to lowest significant bit the word has a 2 bit server ID, a 14 bit Major Period counter and a 32 bit tick counter.

The subsystems in EBEX each have local clocks which are oscillators with stability of 25 parts per million. This means that a subsystem clock can loose or gain one 10 μs tick every 400 msec. To keep the local clocks synchronized to within one tick, the synchronization (sync) message is sent out every 2^{14} ticks which is 163.84 msec (6.1 Hz). The master clock on the time server uses a precision double oven controlled oscillator [35], intended for GPS "hold-over", with a temperature stability of ± 0.2 parts per billion (ppb), between -20C° to +70C°. The aging, 30 days after turn-on, is 0.2 ppb per day, which means that a 1 msec deviation from true elapsed time can occur after $5 \cdot 10^6$ seconds, or 58 days. The jitter in the sync message to sync message latency for a given client-server pair is much lower than one tick. Relative timing of the bolometer and ACS systems is determined by the drift of the local oscillators over the period between sync messages, which is less than 8.2 μs.

The sync message consists of the time servers board ID and the high 32 bits of the time stamp (table 3.1). At the time of the broadcast, the value of the (unsent) low 14 bits is zero. On receipt of a valid sync message the client rewrites its time stamp with the 32 bits received plus 14 zero bits appended. The Board ID is transmitted by the time server to identify itself. The Major Period is incremented only by the servers every six hours even though it has enough bits to count up to 11.9 hrs.

3.2 Time Synchronization Bus

The EBEX timing system is based on local clocks (tick counters) that are kept in synchronization by periodically distributing a synchronization message (time sync) over a serial link called the time bus. The clients on the time bus shown in figure 3.1 are the Attitude Control System (ACS), the Bolometer Readout boards (BRO) and the HWP readout boards. Each of the two time servers in EBEX communicates to the clients through a separate time bus, making two redundant time buses (figure 3.1). Each time bus is implemented as a single differential RS485 pair, driven by the time server. The bit rate on the time bus is 1 Mbit/sec. Manchester encoding [36] is used to encode the data. This bit rate ensures a transition at least twice every micro-second, so that the lowest frequency in a spectrum analysis is 1 MHz.

Each time server transmits the sync messages on its independent time bus. Each client receives both time sync messages but uses the one from the source with the lower ID - the primary server. If, later, this source is not received correctly, the client switches to the other source - the secondary server. If no sync messages are received, the client will continue to increment its tick counter without incrementing the Major Period.

The ACS receives the time sync messages on a designated RS-485 receiver board in the ACS crate which converts it to a TTL[1] signal. The signal is then recorded as a digital channel in the ACS. The BRO and HWP crate each have a timing distribution board with an RS-485 receiver. The timing distribution board receives the time sync messages from the time bus and regenerates them to the Dfmux boards via the backplane of the crate.

3.2.1 CANbus

In addition to the time sync message on the time bus, the time servers also send CANopen SYNC messages on the CANbus. Standard CANopen SYNC messages do not, by default, carry any data. In EBEX, however, six of the available eight data bytes are used to carry the EBEX time stamp. The SYNC message is generated by the ELMB on the time server board. The time server produces SYNC messages at a rate of 5 Hz. These messages include the high 40 bits of the time word (table 3.1). The low 8 bits of

[1] Transistor-Transistor Logic

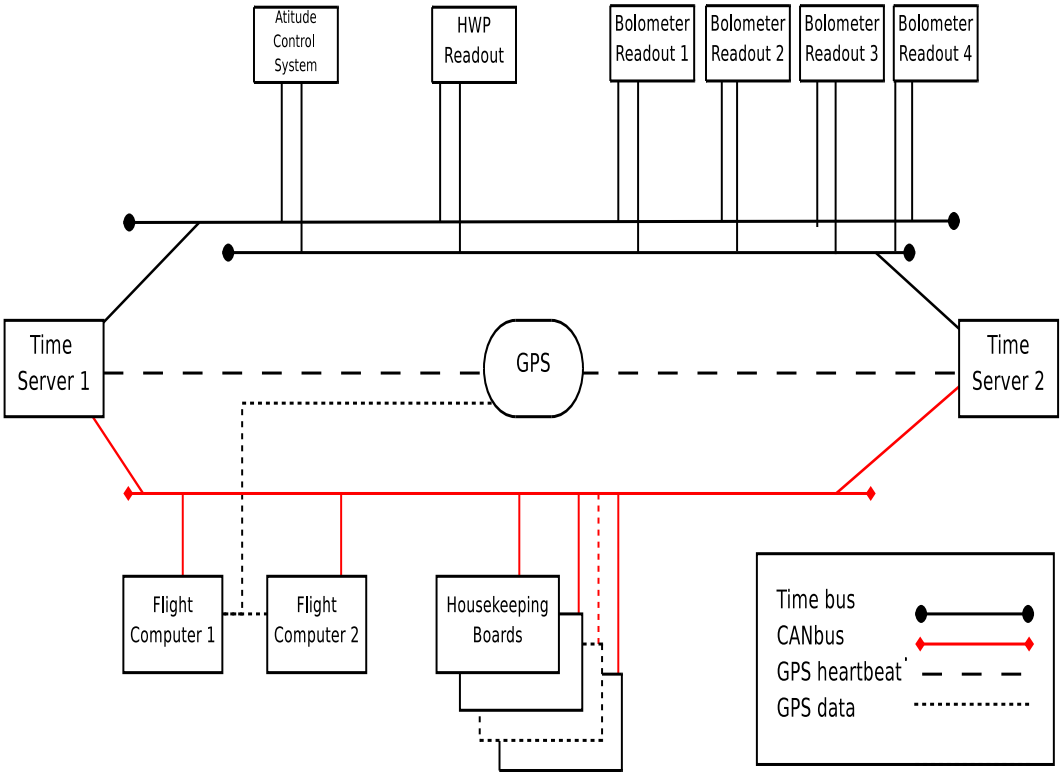

Figure 3.1: The EBEX time bus. The black line represents the RS-485 time buses.

the time word are written as zeros. When an ELMB on any of the cryostat housekeeping boards receives this message, it responds by sampling its channels and writing the data back to the CANbus.

3.2.2 Absolute Time / GPS Heartbeat

Absolute time information is obtained via GPS. The GPS system sends an ASCII absolute time string to the flight computer once a second, via a designated serial interface board. At the same time, it sends a GPS heartbeat pulse with an accuracy of tens of nanoseconds to the time server. The time server then records its current time stamp to disk via CANbus. In this way, the EBEX time stamp is correlated with absolute GPS time. Even in the worst case scenario, where the absolute time is correlated with

the time stamps only once near launch, the stability of the time server clocks should maintain an absolute accuracy of better than 1 msec during a 14 day flight.

3.2.3 The Time bus isolator

The two time servers are physically mounted in different parts of the instrument. Time server 1 is located in BRO1 and is powered by the Cryostat power domain. Time server 2 is located in the flight computer crate and is powered by the ACS power domain (see chapter 6). To prevent coupling of the two power domains, via the common mode of the RS-485 lines of the time bus, opto-isolators are used. A small box containing four channels of isolators is placed between the servers on the bus. The box is mounted on Power crate 1, where both power domains are accessible. The isolator box is not symmetric. On one side of the box there is a time server and the insertion of the GPS heartbeat to both servers. On the other side of the box there is only a time server. Therefore, three channels are input to one side of the isolator and one channel is input to the other side.

3.3 Test Flight Performance

Most of the timing system performed as designed throughout the duration of the test flight. Figure 3.2 shows the Major Period and the time ticks as they were logged by the flight computer. Time server 1 was the primary time server. Its time sync messages were available to all clients throughout the flight. All data samples were properly time stamped. The value of the Major Period was arbitrarily set to 44 and 46 (time server 1, time server 2 respectively), so that they could be told apart in the event of a switch over.

The GPS heartbeat was received by time server 1 but, due to an error in the code, was not correctly logged to disk. Time server 2 did not receive the GPS heartbeat most likely as a result of a hardware failure.

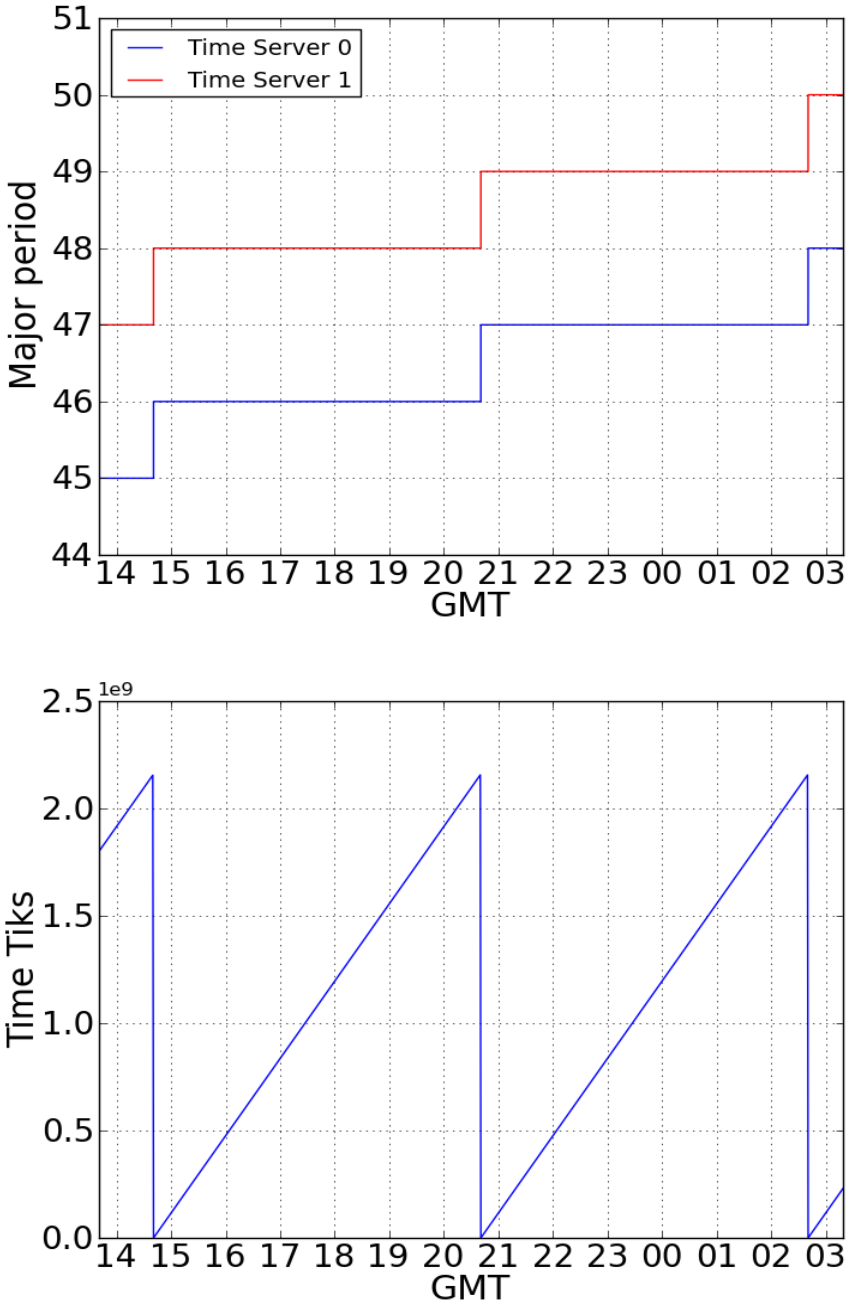

Figure 3.2: Top: The time stamp Major Period during the test flight; Bottom: The Time ticks during the test flight resetting at 6 hrs ($2.16{\cdot}10^9$ ticks).

3.3.1 Bolometers Timing

The Dfmux boards received the time sync message continuously throughout the flight. This is inferred from the fact that there was no switch-over during the flight between the primary and secondary time servers. The time stamped data is sent to the flight computer over the EBEX Ethernet network using multi-cast UDP/IP packets. This communication protocol is considered 'best effort'; some data loss is expected. Excluding a brief period around 17:35 UTC when the Dfmux boards were commanded to reboot during a SQUID tuning procedure, no board is missing more than 65 packets from the logged packet data. This amounts to a total loss rate of $< 0.01\%$.

A synchronization procedure was performed before the test flight to ensure that all the Dfmux boards in a BRO would sample data synchronously. A synchronization between the two BRO was not performed for the test flight. For the Antarctic science flight the synchronization is planned both within each BRO and between BRO's. There was an error in the synchronization of board number 62. As a result, it was sampling out of sync. This error was most likely due to a temporary lack of communication with the board at the time of synchronization procedure.

Figure 3.3 shows the time difference,Δt, between consecutive bolometer time stamps. The sampling frequency of the Dfmux boards was set to 190.73 Hz (25 MHz/2^{17}). This is represented by the red line at 5.2428 msec. The two rows of data points are 10 μsec apart which is one EBEX time tick. The EBEX time stamps and the Dfmux board clock are not synchronized which is why the points do not align with the red line. Nevertheless, the time stamps are always less than 10 μsec from when the data was actually sampled.

3.3.2 ACS Timing

All ACS channels were time-stamped properly. The time sync message was received throughout the flight. ACS_TIMEOK is a flag channel that monitors time sync message reception in the ACS. Its value throughout the flight indicates that the time sync was received continuously. Figure 3.4 shows the difference in time, Δt, between consecutive ACS time stamps. The sampling frequency of the ACS is 100.16 Hz, which is represented by the red line at 9.984 msec. As with the Dfumux boards clock, the ACS clock is not

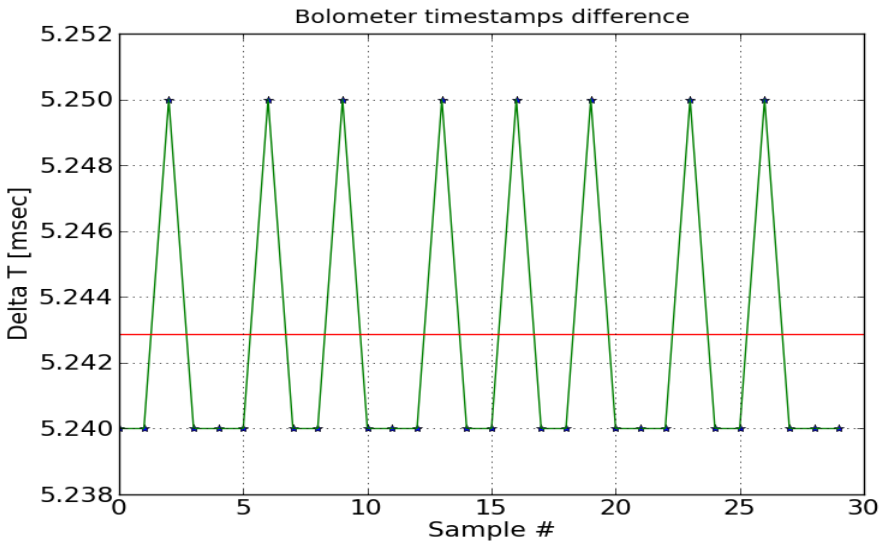

Figure 3.3: The difference in time between consecutive bolometer time stamps. The red line represents 190.73 Hz which the actual data rate of the Dfmux boards.

synchronized with the EBEX time stamps.

3.3.3 CANbus Timing

CANbus SYNC messages were received continuously by the housekeeping boards and the flight computers at 5 Hz throughout the flight. The rate at which the time stamps were written to disk as a slow channel (5.008 Hz) is slightly faster than the rate at which they were produced by the time servers.

When no new data is received within the 5.008 Hz interval the previous data value is written to disk again. Due to this mismatch in rates, periodically the new time stamp would not arrive on time, resulting in two consecutive data samples receiving the same time stamp. Figure 3.5 shows the difference between consecutive time stamp ticks as logged by the flight computer. At a rate of 0.008 Hz (126 sec) two consecutive time stamps have the same value.

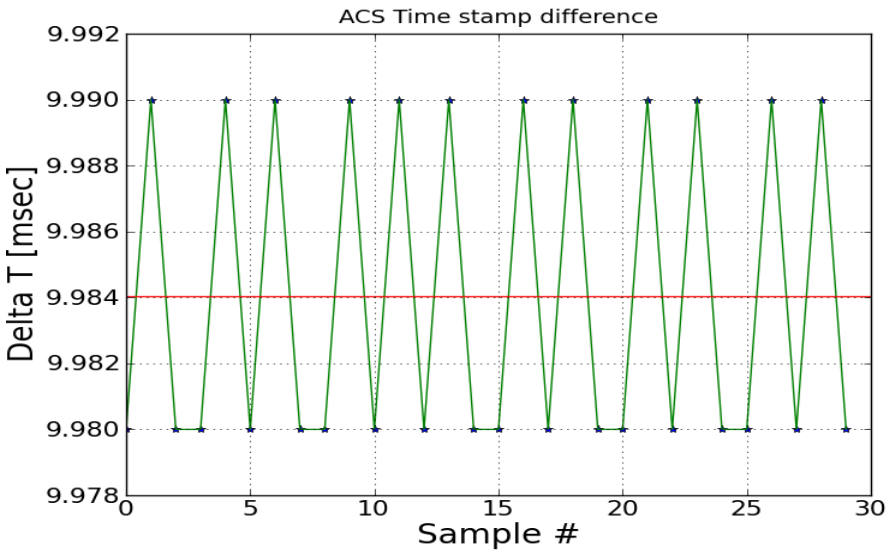

Figure 3.4: The difference in time between consecutive ACS fast time stamps. The red line is at 100.16 Hz which is the data rate of the ACS cards.

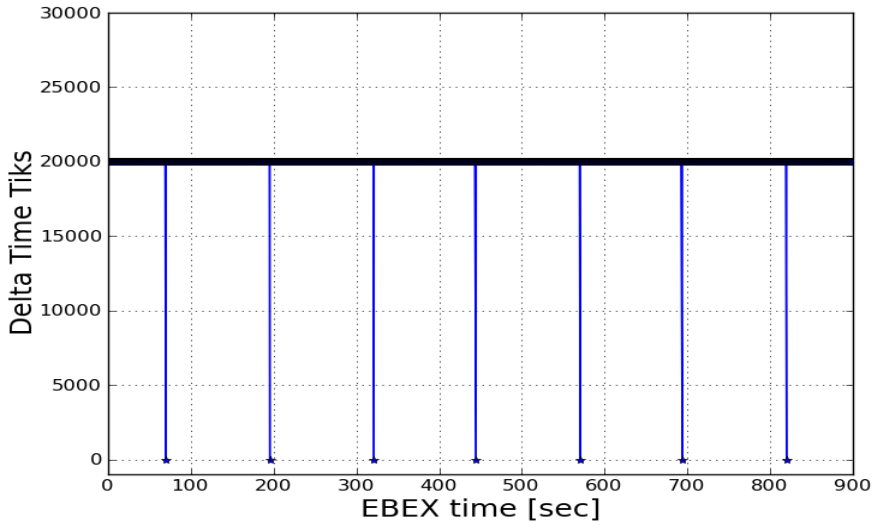

Figure 3.5: The difference between consecutive ticks. Δt=20,000 ticks is the nominal 5 Hz. Δt=0 correspond to a duplicated time stamp.

Figure 3.6 is a histogram of the Δt between consecutive time stamps. The jitter around 0.2 sec is $\pm$20 ticks ($\pm$0.2 msec). This jitter can be explained by the fact that the CANbus time stamp only included the highest 40 bits of the EBEX time word (see table 3.1). The lowest 8 bits were appended zeros, resulting in an uncertainty of 0.25 msec.

CANbus dropped samples

Figure 3.7 shows the Δt between consecutive CANbus time stamps during the test flight. Most Δt are close to 0.2 sec, corresponding to the nominal 5 Hz. When two samples receive the same time stamp, the next time stamp will have Δt=0. Nevertheless, some time stamps were dropped, resulting in a $\Delta t \geq 0.4$ sec. This became significantly worse during the bolometer tuning when a script called keepFP800 was running on the flight computer. The red vertical lines in figure 3.6 mark the times when this script was started and stopped.

The script keepFP800 starts a new thread that reads CANbus messages from the USB-to-CANbus message buffer. The additional thread causes the main CANbus thread, monitorCAN (see section 4.3.1) to miss some messages. Outside of the time when this script was running a total of 184 time stamps were dropped which are less than 0.06% of all the logged time stamps.

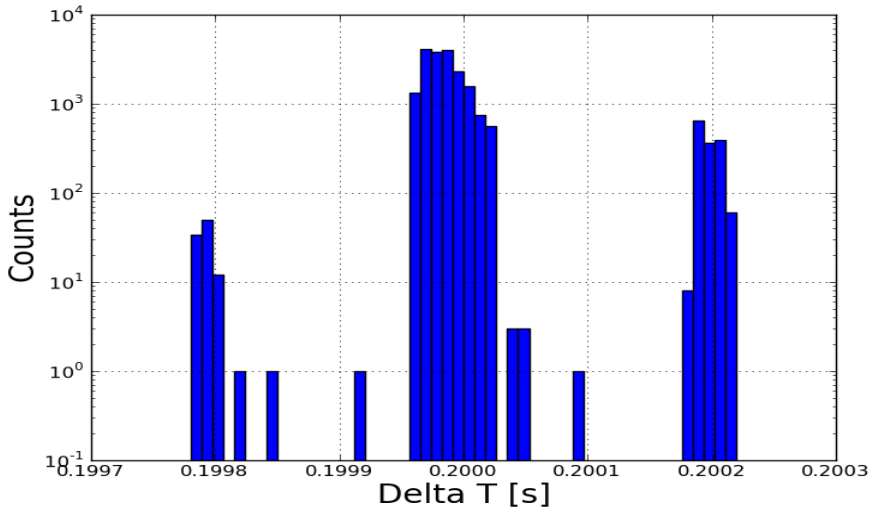

Figure 3.6: Histogram of the difference in seconds between consecutive CANbus time stamps.

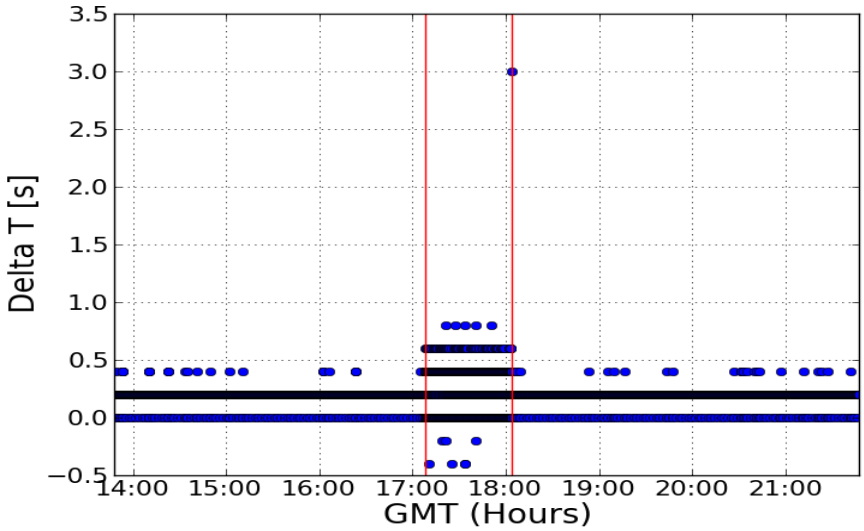

Figure 3.7: The difference between consecutive time stamps. The vertical red lines mark time that keepFP800 was running.

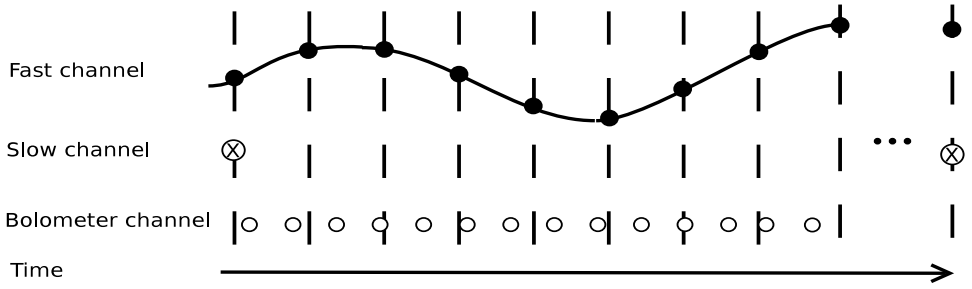

Figure 3.8: The black curve represents data from an ACS sensor. The black filled circles show the fast sample rate. Circles with an 'X' represent a slow sample rate. Empty circles represent the bolometer sample rate. The dashed lines are aligned with the fast sample rate.

3.3.4 Data Alignment

The various subsystems record data at different rates. A pictorial representation of the data sampling rates is shown in figure 3.8. All the ACS channels sample synchronously. Every twenty fast samples, the slow channels are sampled. In order to align the data, a linear interpolation between every two ACS data points is performed. The data value corresponding to the nearest bolometer sample time is found (figure 3.9). This process is repeated for every bolometer time stamp, effectively resampling the 100.16 Hz fast ACS channel into a 190.73 Hz channel. Chaoyun Bao did a calculation estimating the error associated with this process by resampling a sinusoidal test signal from 100.16 Hz to 190.73 Hz using linear interpolation. Figure 3.10 shows the maximum error between the resampled data and the original signal. For signals with frequencies lower than 20 Hz the maximal error from the data alignment is less than 1.5%.

3.3.5 Future plans

A test for measuring the latencies between time stamps at the various subsystems is planned. An external signal will be inserted into all clients simultaneously, including an optical signal for bolometers. Time stamps of the resulting signals will then be compared. The latencies of each client may vary, but are expected to be lower than the desired timing accuracy. If needed, latencies could then be compensated for.

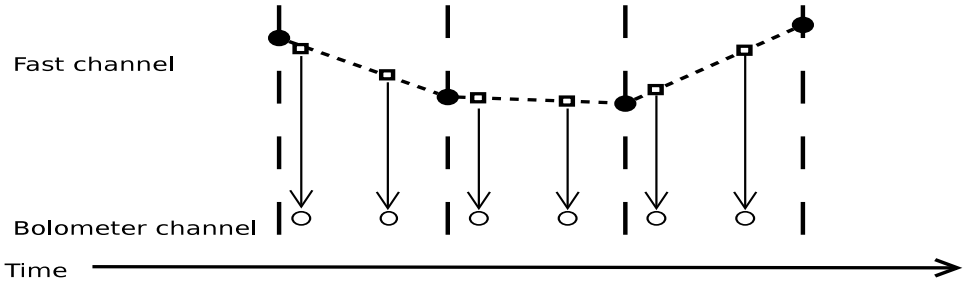

Figure 3.9: A close up view of fast ACS data and bolometer data. The dotted line represents the linear interpolation between the data point of the ACS channel (black circles). The squares represent the interpolated value at the time of the bolometer samples.

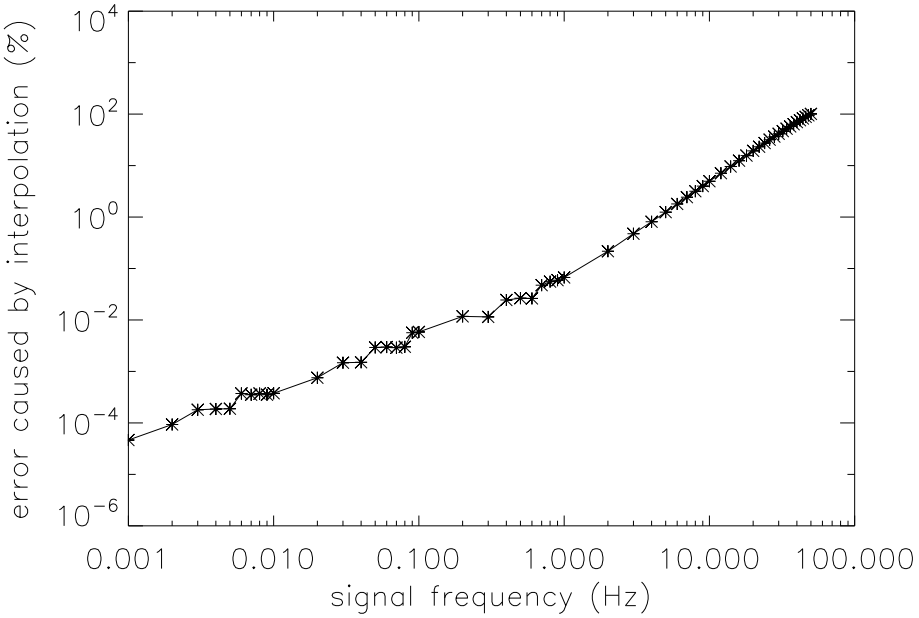

Figure 3.10: Error in linear interpolation vs signal frequency (Plot by Chaoyun Bao).

Chapter 4

Housekeeping Electronics

Four novel boards were developed for the purpose of monitoring and controlling the temperatures of the various temperature stages of the EBEX cryostat. These boards were developed by our collaborators at the Weizmann Institute of Science. The housekeeping boards measure the temperature of the sensors and control the heaters and heat switches of the adsorption refrigerators. The boards are interconnected and controlled over a Controller Area Network (CANbus) [37].

I tested and integrated the boards and the related software. I analyzed the temperature data and characterized the cryogenic performance of the adsorption refrigerators and assessed the performance of the boards during the test flight.

4.1 CANbus and ELMB

CANbus is a high-reliability, low speed, 2-wire serial bus standard for industrial control. It is a message based protocol, designed originally for automotive applications but now also used in other areas such as industrial automation and medical equipment.

Each node on the bus requires a host processor which decides what messages it will transmit and what the received messages mean. In EBEX this is performed by the ELMB,[1] a general purpose I/O microprocessor plug-on daughter board with CAN interface. The ELMB was developed for the ATLAS experiment at CERN [38] and is radiation tolerant [39], making it suitable for balloon and space applications. It

[1] Embedded Local Monitoring Board

has a 4 MHz processor[2] with 128 kBytes of on-board flash memory and 4 kByts of EEPROM.[3] CANopen [40] is a higher level communication protocol used in EBEX to control the nodes and maintain communications on the CANbus. The software is described in section 4.3.1.

When a message is sent on the CANbus, it has an ID which specifies the target recipient node. All nodes see all the messages on the bus but only the recipient node responds to it. When a node starts to send a message, it first verifies that no other node is trying to send a message at the same time. Node IDs range from 0-63; the higher the node ID number, the higher is that node's priority. Depending on its priority, the node either continues sending the message or stops and tries again at the next opportunity.

Typically, the CANopen SYNC message does not carry any data. Custom firmware for EBEX ELMB uses the SYNC message to send the time stamp (see chapter 3) to the nodes. When a SYNC message is received by the node, it performs a sequence of measurements of the channels on the board. The node then writes the digitized voltage values back to the CANbus, together with the time stamp of the SYNC message that triggered the measurement. The flight computer parses the data messages from the boards and writes it to disk.

Figure 4.1 is a schematic representation of the EBEX CANbus. The CANbus is configured to run at a rate of 500 kbit/sec and is terminated at its ends with 110 Ω resistors. The two flight computers are connected to the CANbus via CANbus-to-USB interfaces [41].

As described in chapter 6, EBEX has two isolated parallel power systems. Some housekeeping boards are mounted in BRO1 which is powered by the Cryostat power system, while some boards are in the flight computer crate which is powered by the ACS power system. In order to prevent coupling of noise and grounding loops between the two power systems by the CANbus, optical repeaters [42] are used to break the electrical continuity of the CANbus. The signals on the CANbus are transferred over optic fiber (figure 4.1) and the two power systems remain electrically isolated from each other.

[2] ATmega128

[3] Electrically Erasable Programmable Read-Only Memory

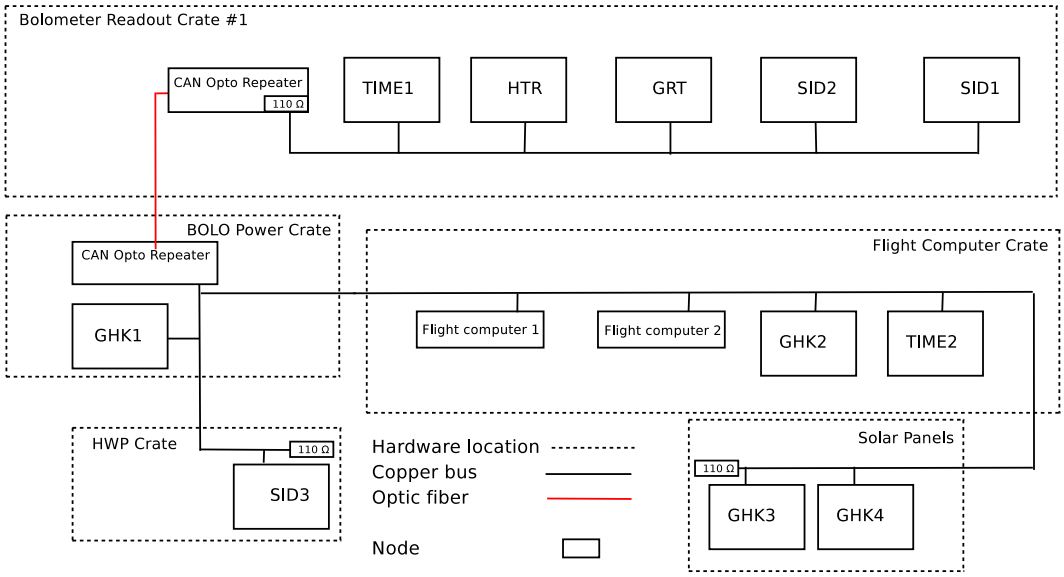

Figure 4.1: A diagram of the EBEX CANbus. The two optically isolated parts of the CANbus are powered by separate power domains.

4.2 Housekeeping Boards

The housekeeping boards use analog to digital converters [43] (ADC) for measuring voltage. The voltage can be either the output of a sensor or the voltage across a sense resistor. Some properties of the housekeeping boards are given in table 4.1.

Board Name	# of boards in EBEX	# of Channels (Analog)	#Channels (Digital I/O)	Power [W] per board
Silicon Diode	3	16	-	0.7
Heater	1	8	4	0.75
Germanium/Ruthenium	2 [1]	7 [15]	-	1.6
General Housekeeping	2 [4]	64	24	1
Time Server	2	-	10	1.5

Table 4.1: Number of channels on EBEX housekeeping boards. For the Germanium Ruthenium board the value given in square brackets is for the science flight.

4.2.1 General Housekeeping board

Two types of ELMBs are used in EBEX. One has a built-in ADC (typically A series); the other does not. The General Housekeeping board (GHK) must have an ELMB of the first type as it is an interface board for using the built-in ADC. This 16 bit ADC has a sample rate set to 15 Hz which is significantly slower than the ADC used on the other housekeeping boards. This means the GHK board may take several seconds to sample all its channels. Therefore the GHK board ELMB is configured to respond to every 40^{th} SYNC message. Consequently, the GHK starts a measurement sequence every eight seconds.

The GHK channels are divided into several groups. Two channels are designated for reading out liquid helium level sensors. Ten other channels are on connectors intended for the disk pressure vessel (see chapter 5) temperature and pressure sensors. The other 52 channels are accessible by five connectors on the board. These are split in the following way: 20 channels are designed to read out AD590 [44] temperature sensors; 20 channels are designed to readout differential voltage; and 12 additional channels can be set by jumpers to either of the two modes.

Due to a layout error on the GHK board the ADCs were unusable during the test flight. The digital I/O channels on GHK1 (see figure 4.1) were used to control solid state relays that routed power to various parts of the HWP system and to inhibit bolometer power. These features were used reliably during the pre-flight integration and were used to re-grip the half wave plate (HWP) at the end of the flight.

During the Antarctic flight two additional GHK boards will be used to monitor temperatures and voltages of the solar panel and battery charging system.

4.2.2 Silicon Diode Board

The Silicon Diode board (SID) is designed to readout diode temperature sensors. In EBEX silicon diodes [45] are used to measure temperatures between 1.5°K and 300°K. The board is capable of making a four-wire-measurement of a diode's voltage in the range 0 - 2.5 V. In EBEX, in order to minimized cryogenic wiring, only two wires per sensor are used. Each channel has a separate 10 μA DC excitation current, while voltage is read out by two 16-bit ADC. The input to the ADC is controlled by an 8 channel

multiplexer. The multiplexer and the ADC are controlled by the ELMB. The excitation current, which dissipates less than 15μW per sensor, remains continuously on.

In the EBEX cryostat two diodes are mounted on the top and two on the bottom of each of the four shells (VCS2, 77K, VCS1, 4K). Several other sensors are mounted around the cold plate. The adsorption refrigerators have diode temperature sensors built-in to the heat-switches, pump heaters and the 4°K base plate. The HWP assembly has six sensors mounted at various positions. The SID board which reads out the HWP sensors is mounted in the HWP crate. It is separate from the other housekeeping boards (see Fig. 4.1).

Due to a firmware mismatch on the HWP SID board the temperature sensors on that board were not read out during the test flight. Several of the shell diodes were not read out due to wiring problems in the cryostat.

Ground data

The SID boards were calibrated using a diode immersed in liquid nitrogen. The results are shown in table 4.2. As a consequence of this calibration an offset of 20 mV was subtracted from all SID channels before converting the voltage to temperature.

Figure 4.2 shows 2 hours of data from a sensor mounted on VCS2. The data was recorded before launch when the gondola and cryostat were stationary. The value of 0.817 V $\pm$ 4 mV corresponds to a temperature of 184°K $\pm$ 2°K. Figure 4.2 shows the power spectrum of the same data after subtracting the average. The power spectrum is flat.

4.2.3 Germanium/Ruthenium Temperature Board

The Germanium/Ruthenium Temperature (GRT) board was designed for measuring sub-Kelvin temperatures in EBEX. The sensors used in EBEX are Ruthenium dioxide temperature sensors [46]. The GRT board performs a 4-wire measurement of the sensor's resistance. In addition, it has a built-in sensor which measures the board's temperature. The sensors are excited by a square wave at a frequency of 250 Hz. The voltage output is then demodulated, filtered and digitized. The excitation of the sensor dissipates little power at the sensor. For example, when the temperature of the sensor is $\sim$280 mK

Channel	Voltage[V]	± mV	ΔV
0	1.002	1	25.5
1	1.005	3	22.5
2	1.006	2	21.5
3	1.009	3	18.5
4	1.008	2	19.5
5	1.007	2	20.5
6	1.007	3	20.5
7	1.008	1	24.5
8	1.007	1	16.5
9	1.009	3	18.5
10	1.012	2	15.5
11	1.014	2	13.5
12	1.006	1	21.5
13	1.008	2	19.5
14	1.011	2	16.6
15	1.007	3	20.5

Table 4.2: Calibration data from SID2 at 77°K. At 77°K the diode should read 1.0275 V.

its resistance is ∼6 kΩ. This means the power dissipated by the excitation is 60 pW. At higher temperatures the resistance of the sensor is lower and therefore less power is dissipated.

In EBEX two boards measured the temperatures of the two adsorption refrigerator's cold stages, the temperatures of the bolometer wafers, the focal plane structure and the 1°K cold optics (see figure 2.6).

Capacitive Filters

Capacitive filters were used to preserve the RF integrity of the cryostat (see section 2.5.5). The filters were installed at two locations along the signal path between the board, mounted in BRO1, and the sensors. One location is at the cold plate which is at a temperature of 4°K. The other location is at the 'tin can' an RF tight cylinder at the bottom of the cryostat (see section 2.5.5). The capacitance is between the signal line and the cryostat shell, which is grounded to the board's power return (see figure 6.1). This

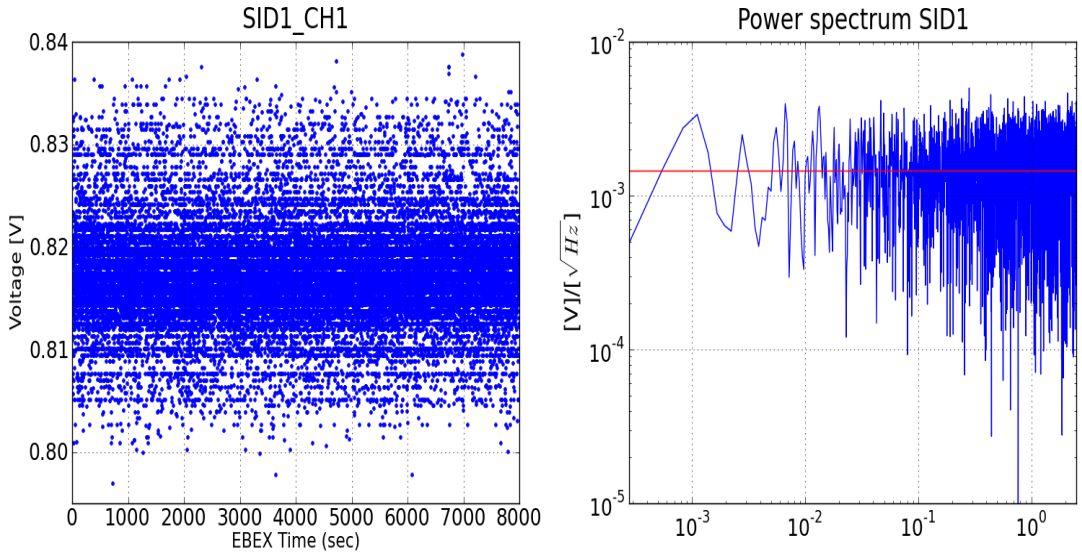

Figure 4.2: Raw data (left) and Power spectrum (right) from a SID channel in EBEX in the lab.

affects the output of the board mostly at high resistance values as shown in figure 4.3.

New GRT

A new version of the GRT board was produced after the test flight. The new board has 15 channels as well as a board temperature sensor. The excitation frequency was changed from 250 Hz to 161 Hz. Several other improvements were implemented such as making the measurement differential. The new board has been successfully integrated into EBEX. A single board is now used instead of the previous two.

Ground data

Figure 4.4 shows 30 minutes of data from a sensor mounted on the focal plane. The data was taken before launch when the gondola and cryostat were stationary. The value of 40500 $\pm$ 350 ADC counts corresponds to a temperature of 280.9 mK $\pm$ 3 μK. Figure 4.4 shows the power spectrum of the same data after removing the average. The power spectrum shows excess noise between 0.05 Hz and 0.14 Hz. Several possible sources,

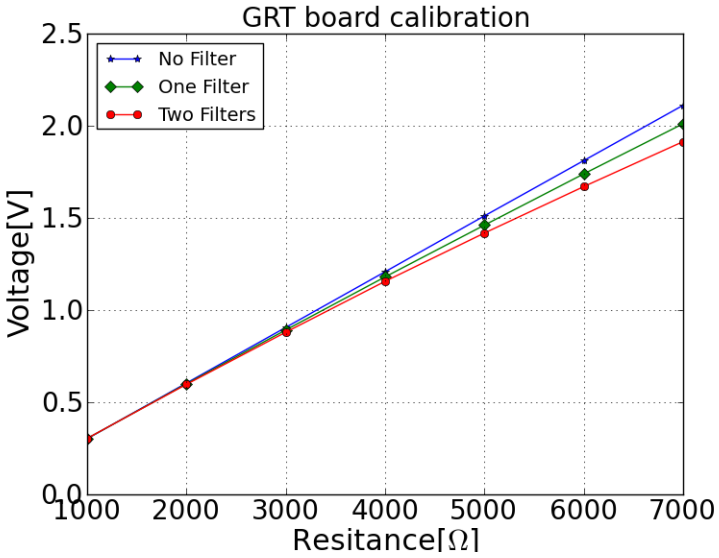

Figure 4.3: The capacitive filters were in the signal path of the GRT board outside of the cryostat. Test resistors were used while the capacitors were connected with a grounding strap to the cryostat.

such as gondola pendulations and temperature fluctuations, were investigated and ruled out as the cause of this noise. The source of the noise remains unknown. The flight data is shown in section 4.4.

4.2.4 Heater Board

The adsorption refrigerators are used to cool the detectors and optics inside the cryostat. They implement carbon pumps with heater elements and gas-gap heat switches that control the conductivity between the pumps and the 4°K base plate. The heater board is used to control these elements and cycle the refrigerators. The board has eight channels designated for pump heaters and six channels for gas-gap heat switches. Each heater channel has three states: High (0 - 24 V), Low (0 - 6 V) or Off. The value of each state is set by a potentiometer. Each heat switch channel can be preset to an output voltage of up to 5.5 V. The state of each heater or heat switch channel is determined by a solid state relay which is controlled by a programmable logic device (PLD). The PLD is

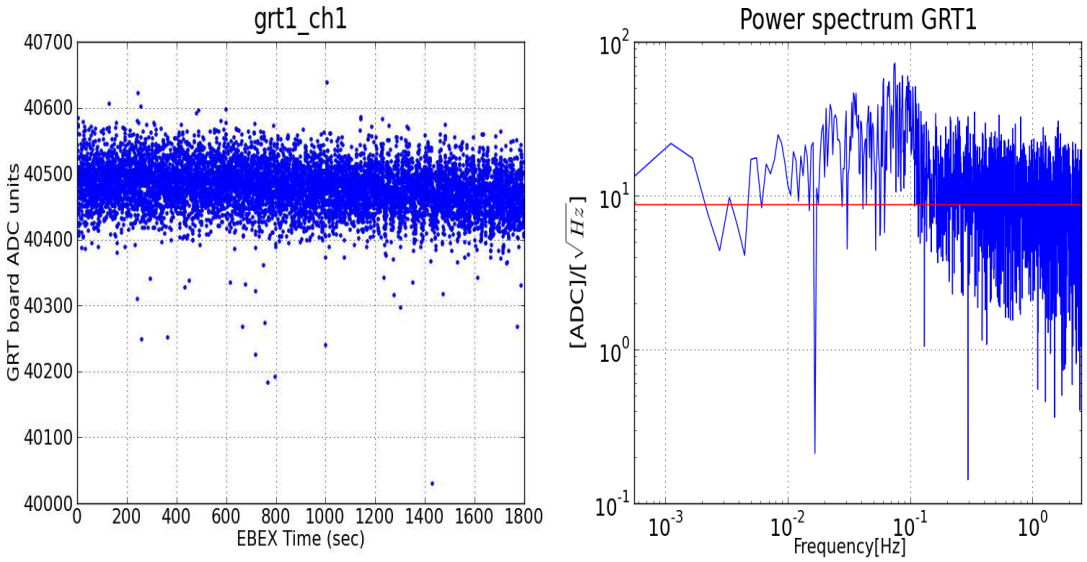

Figure 4.4: Raw data (left) and Power spectrum (right) from a GRT channel in EBEX in the lab.

controlled by the ELMB microprocessor which receives the refrigerator state command from the flight computer over the CANbus. An external DC/DC board supplies power (13 V/26 V) for the heater channels. All output currents are monitored via a sense resistor and are read out over the CANbus.

The heater board was used in the test flight to warm up the focal plane during the bolometer tuning. Commands were reliably carried out.

4.2.5 Time Server

In addition to its operating as a server for the EBEX time bus, the time server board is also a node on the CANbus. Its primary purpose as a time server is described in chapter 3. In addition, the time server board has ten digital output channels, eight of which are used to send commands to the Dfmux boards via the timing distribution boards and the crates backplane. These commands include a 'hard' FPGA reset command, a software reset command and a command to power on/off an individual crate.

During the integration several problems were found with the commanding of the

Dfmux boards via the time server board. The boot-up state of the time server's digital output channels was such that a command was initiated every time the board's power was cycled. In addition some lines were unstable causing reset commands to be issued randomly. As a result, some Dfmux boards became non-responsive. Due to these problems the time server's digital outputs were not used in flight and the cable was left unplugged.

This failure prompted the design of a new board which was designed by colleagues at McGill University. The new board requires a clocked sequence of bits in order to carry out a command. There is also an auxiliary voltage output used in EBEX to power a fan inside the crate. The new board provides the 25 MHz clock to the Dfmux board and distributes the time sync via the backplane. The new timing distribution board has been tested and integrated.

4.3 Code

4.3.1 monitorCAN

The flight control program (fcp) has a dedicated thread for managing the CANbus called monitorCAN. This thread, schematically displayed in figure 4.5, is started when fcp starts. First, the computer establishes communication with the USB-to-CAN adapters and sets bus parameters. Next, each node is initialized and its unique settings are confirmed. At the end of the initialization sequence the nodes are set to operational mode so that they are ready to measure and transmit data. The last boards to be set to operational mode are the time servers. Once operational, both time servers start transmitting SYNC messages to the bus.

When the initialization is completed, monitorCAN enters a continuous loop where it reads every CANbus message and translates it. The translation means checking which node the message is from, extracting the data from the message and writing it to the appropriate memory channel to save to disk. The data is stored in ADC counts. On the ground station computer the counts are converted to voltage and then to temperature, using a lookup table. Error messages are written to the fcp log file. Both flight computers read and interpret all the CANbus messages but only the computer 'In charge', as determined by the watch-dog card, can write messages to the bus.

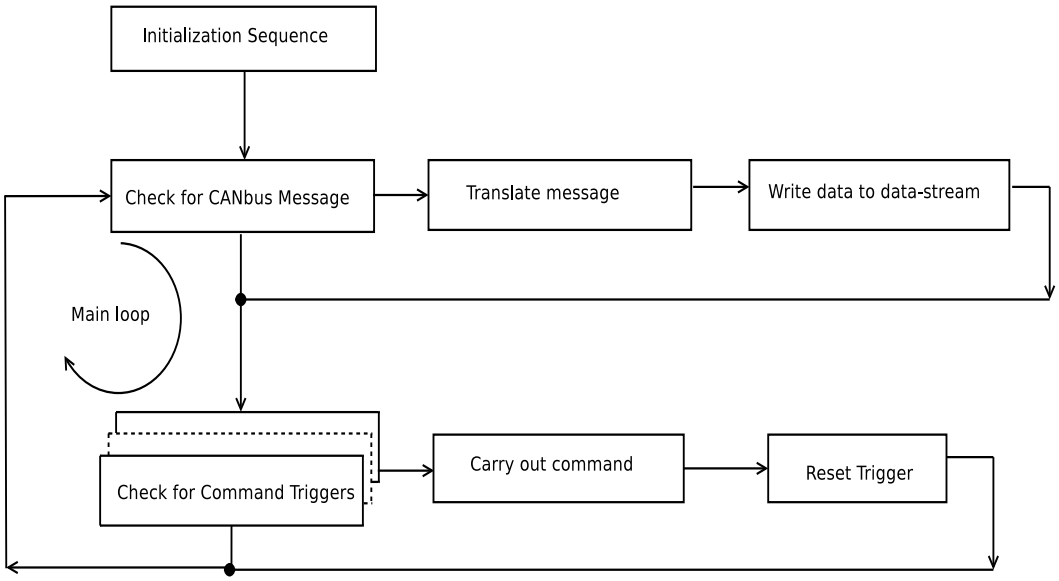

Figure 4.5: A block diagram describing the operation of the monitorCAN thread in fcp.

The monitorCAN thread, once in its main loop, continuously checks for triggers for the various commands issued to boards via CANbus. Examples for such commands are turning on or off a heater board channel, turning on the HWP laser encoder or powering down a BRO. There are a total of 37 such commands.

Some of the commands that are triggered by monitorCAN start an additional branch thread. These include a script that cycles the refrigerators and a script that warms the focal plane to a temperature of 800 mK at which the detectors can be tuned. Both scripts rely on temperature data read from the CANbus for feedback.

4.4 Test Flight

The performance of the cryostat housekeeping electronics during the test flight was assessed. Figure 4.6 shows test flight temperature data from sensors on the focal plane, the optics box, the He8 refrigerator cold head and the RF tower 400 mK stage. Vertical lines mark the launch (red-solid), the beginning and the end of bolometer tuning (black-dash), the planet-like scan (blue-dots), the wide slew scan (red-dash-dot) and the dipole

scan (green-dash). During the bolometer tuning the focal plane was heated to 800 mK.

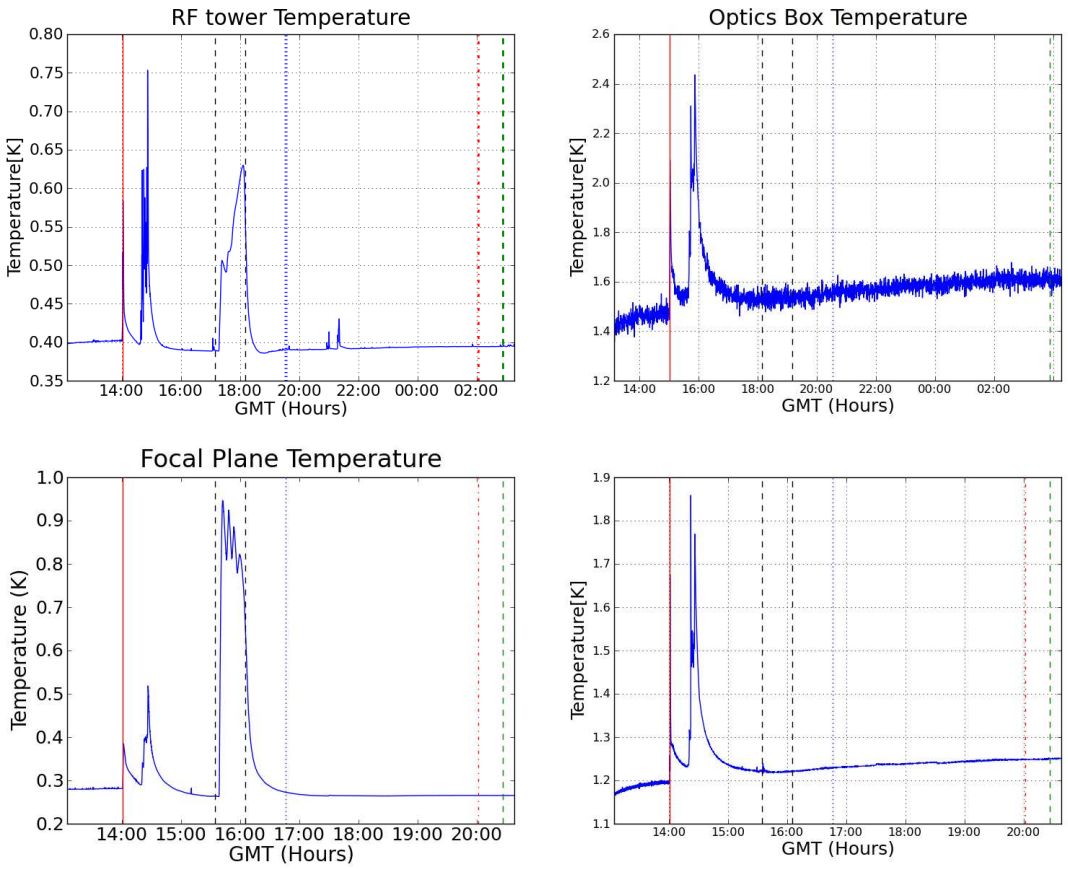

Figure 4.6: Flight data measured with the housekeeping boards. Major events during the flight are marked with vertical lines.

Figure 4.8 shows the temperature of the EBEX cryostat shells during the flight. The nitrogen tank temperature is stable since it contains liquid nitrogen throughout the flight. The helium tank is also stable. There is a spike in the temperature of the helium stage of $\sim$0.3°K during the bolometer tuning when power was applied to the focal plane.

As the balloon ascends the temperature of the readout boards changes by $\sim$ 15°C (figure 4.7). The effect of this change in temperature on the readout can be probed by checking a current-sense channel from the He8 heat switch. The heat switch channel

was continuously on throughout the flight. Figure 4.7 shows clear correlation between the output current and the temperature in the crate. If the all the change in current-sense output is attributed to the change in temperature then it is a 0.2% effect. Such an effect is not observed in temperature readout channels (see figure 4.8).

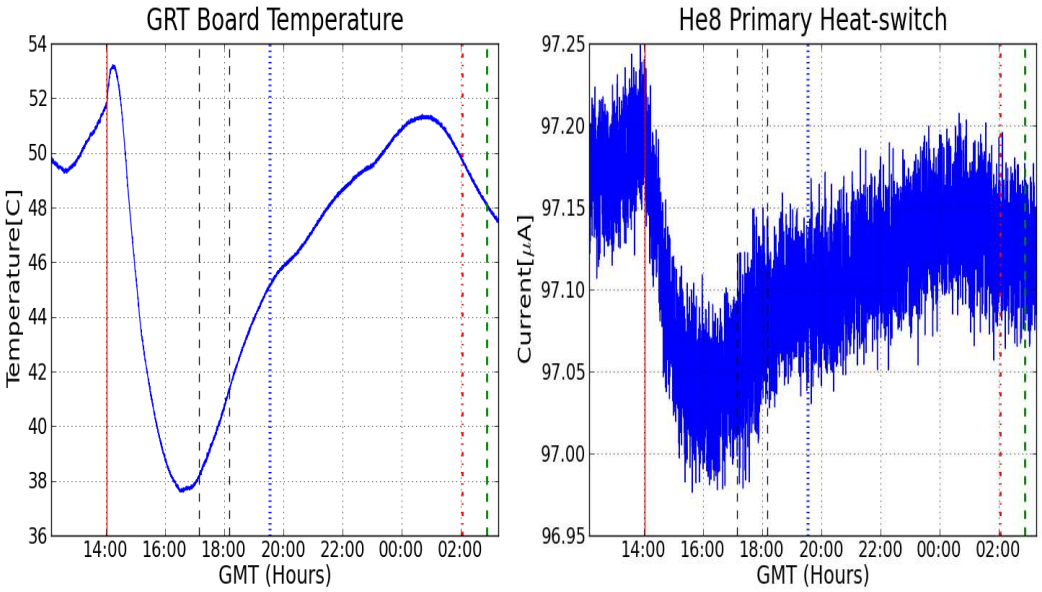

Figure 4.7: Temperature inside the BRO as measured by a sensor mounted on a GRT board (left) and He8 heat switch current sense (right). The temperature drops as the balloon passes through the tropopause, then increases at float and decreases again at 00:29 GMT, as the sun sets.

The temperature of VCS1 is inversely related to the power load on the liquid helium stage. When the load on the 4°K stage increases, this results in a higher boil-off rate of liquid helium, which causes more helium vapor to cool VCS1. So, with a higher load on 4°K, the temperature of VCS1 decreases and visa-versa. When the instrument reached floating altitude the load on helium stage decreased and the temperature of VCS1 increased by ∼1°K. The drop in VCS1 temperature at ∼ 18:00 occurred when the bolometer tuning was completed and the focal plane was cooled, thus momentarily increasing the power load on the 4°K shell. VCS2 temperate decreases as the cryostat's outer shell cools.

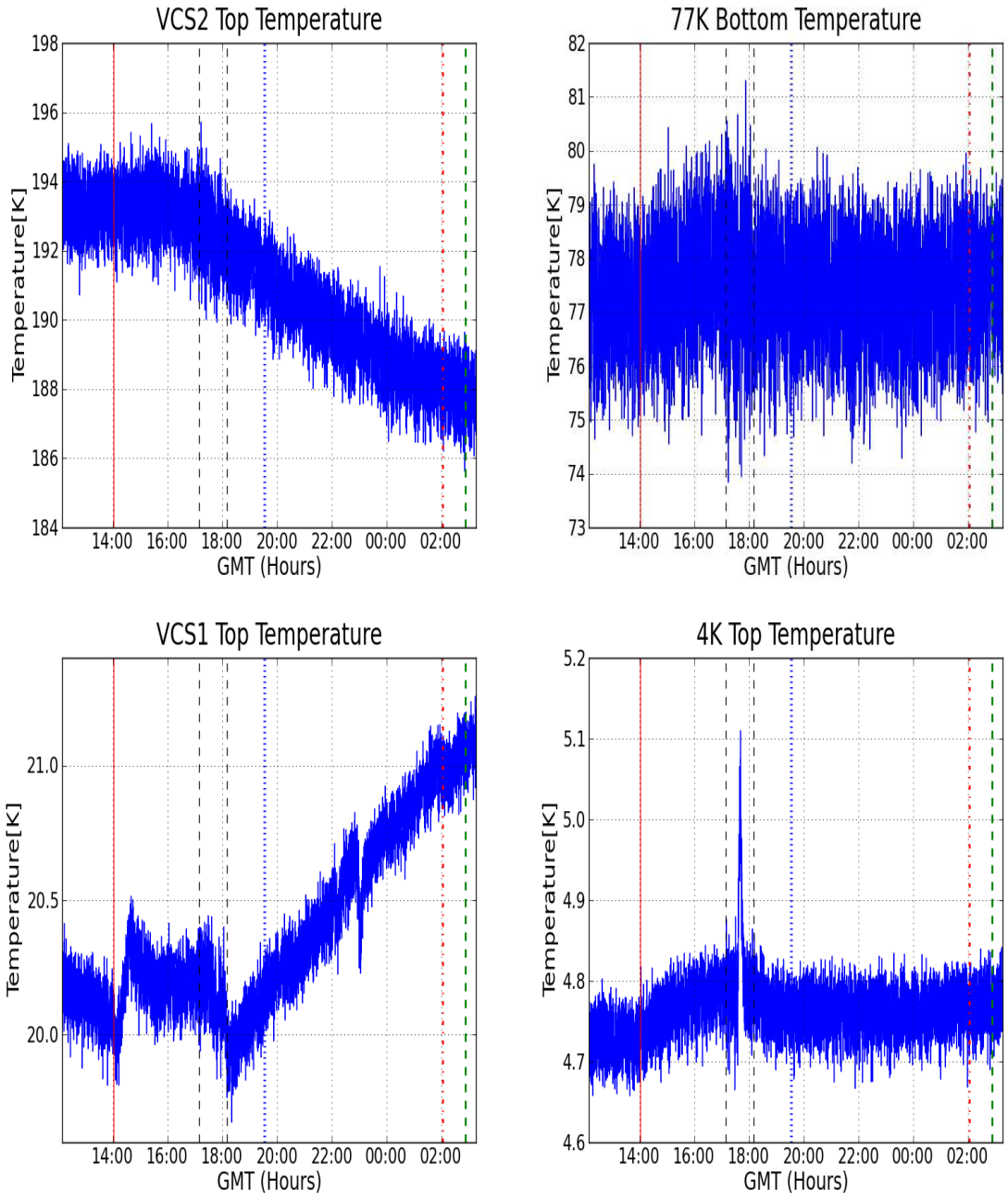

Figure 4.8: Data from cryostat shells temperature sensors during the test flight.

4.4.1 Scan Synchronous Signal

'Planet' scan

A scan of Saturn was planned as an absolute calibration of the responsivity of the bolometers. However, due to poor performance of the real time pointing, Saturn was not in the field of view during the scan. Nevertheless, a planet-like scan was performed. Figure 4.9 shows the azimuth of the gondola during this scan. The amplitude of the scan was $\sim 6^\circ$ and the frequency was 0.045 Hz. An analysis was performed to search for scan synchronous signals in the cryostat temperatures. Any such signals would be sinusoidal-like with a period of twice the scan size. An offset and slope were subtracted from the temperature data before binning it into 12 azimuth bins. Any model which gives a reduced $\chi^2 > 2.32$ is rejected with 99% confidence level.

Figure 4.10 shows data from the refrigerator cold heads binned in azimuth. The He10 cools the focal plane while the He8 cools the cold optics (see figure 2.6). An upper limit of $69^\circ\mu$K on the peak-to-peak amplitude of any scan synchronous signal in the focal plane temperature was set. Similarly an upper limit of $365^\circ\mu$K was set on scan synchronous signal in the cold optics.

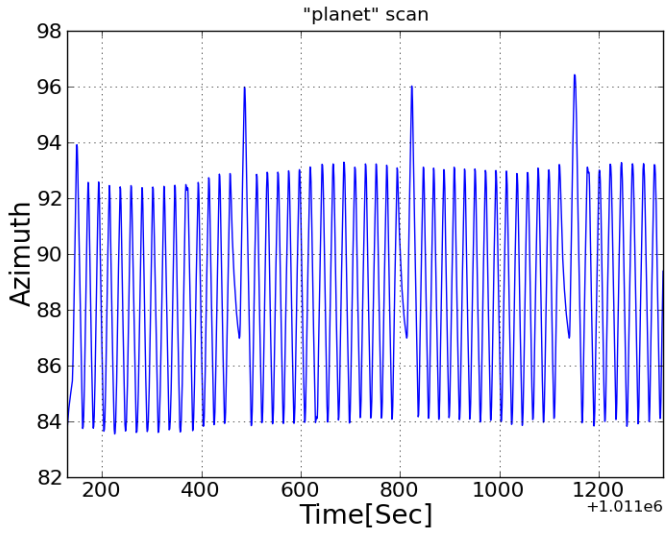

Figure 4.9: Gondola azimuth during the planet-like scan.

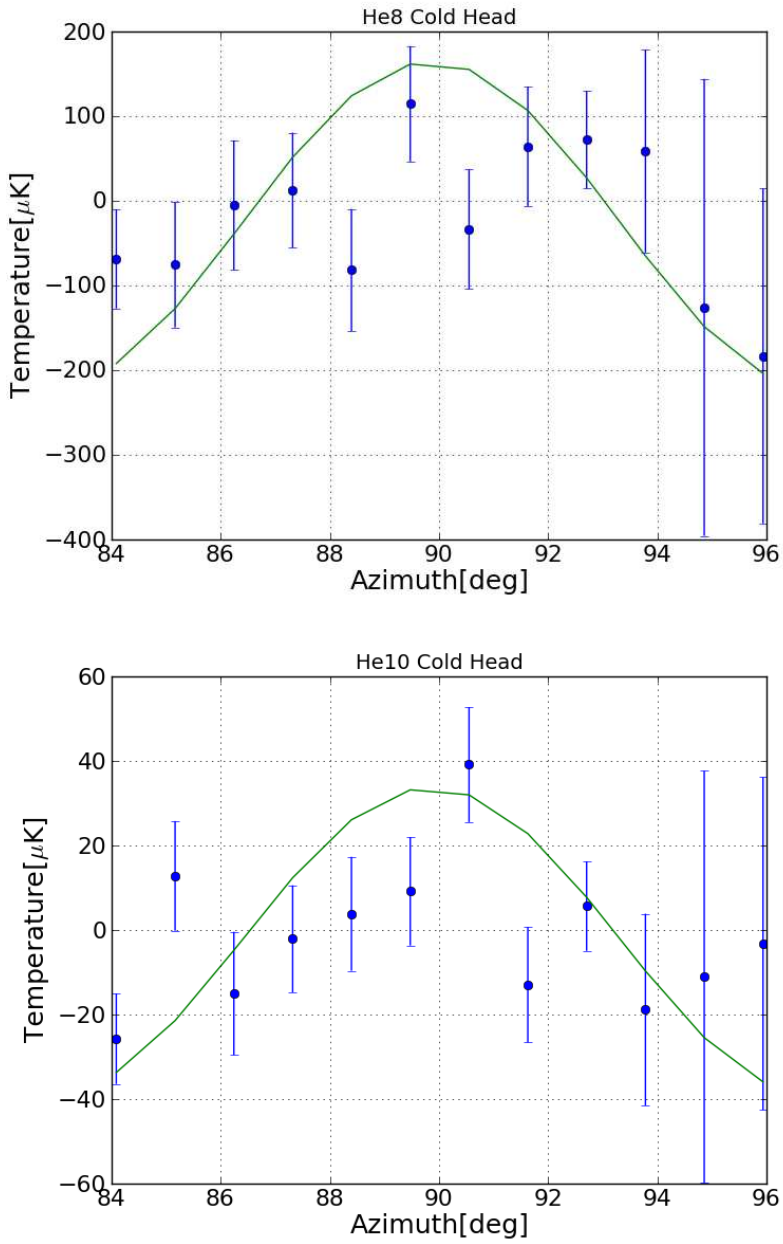

Figure 4.10: Temperature of the refrigerator cold heads during the planet-like scan binned in azimuth. The He8 (top) cools the optics box and cold optics; The He10 (bottom) cools the focal plane. The green line is the fitted model with the highest amplitude that can not be rejected.

Wide slew Scan

A wide slew scan was performed in the anti-sun direction in order to characterize the instrument's far sidelobes. The azimuth of the gondola during this scan is shown on the left hand side of figure 4.11. The right hand side is a power spectrum of the azimuth data. The wide slew scan was at a scan speed of 0.5°/sec, and the peak to peak amplitude ranged from 60° up to 120°.

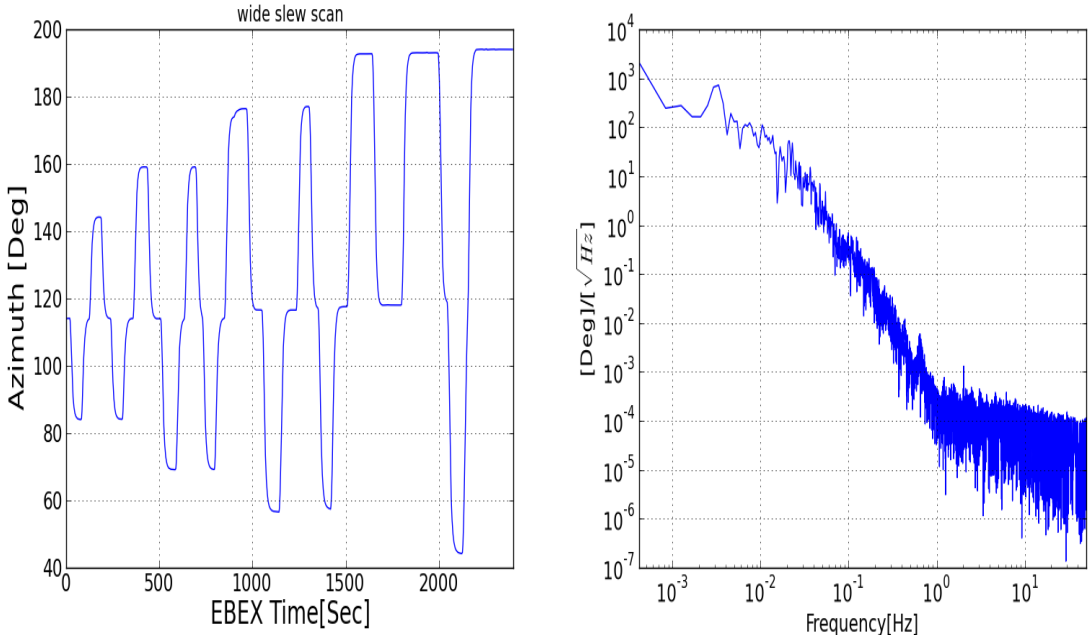

Figure 4.11: Left: Azimuth of the gondola during a wide scan. Right: Power spectrum of the azimuth data.

The search for scan synchronous signal was done by plotting the power spectrum of the temperature data and checking for any signal at the frequencies corresponding to the scan (0.003 Hz.and 0.65 Hz). Figure 4.12 shows the temperatures (left) and power spectra (right) of the 410 GHz wafer and the optics box sensors. Both spectra are flat down to a mili-Hertz, exhibiting no detectable scan synchronous signal.

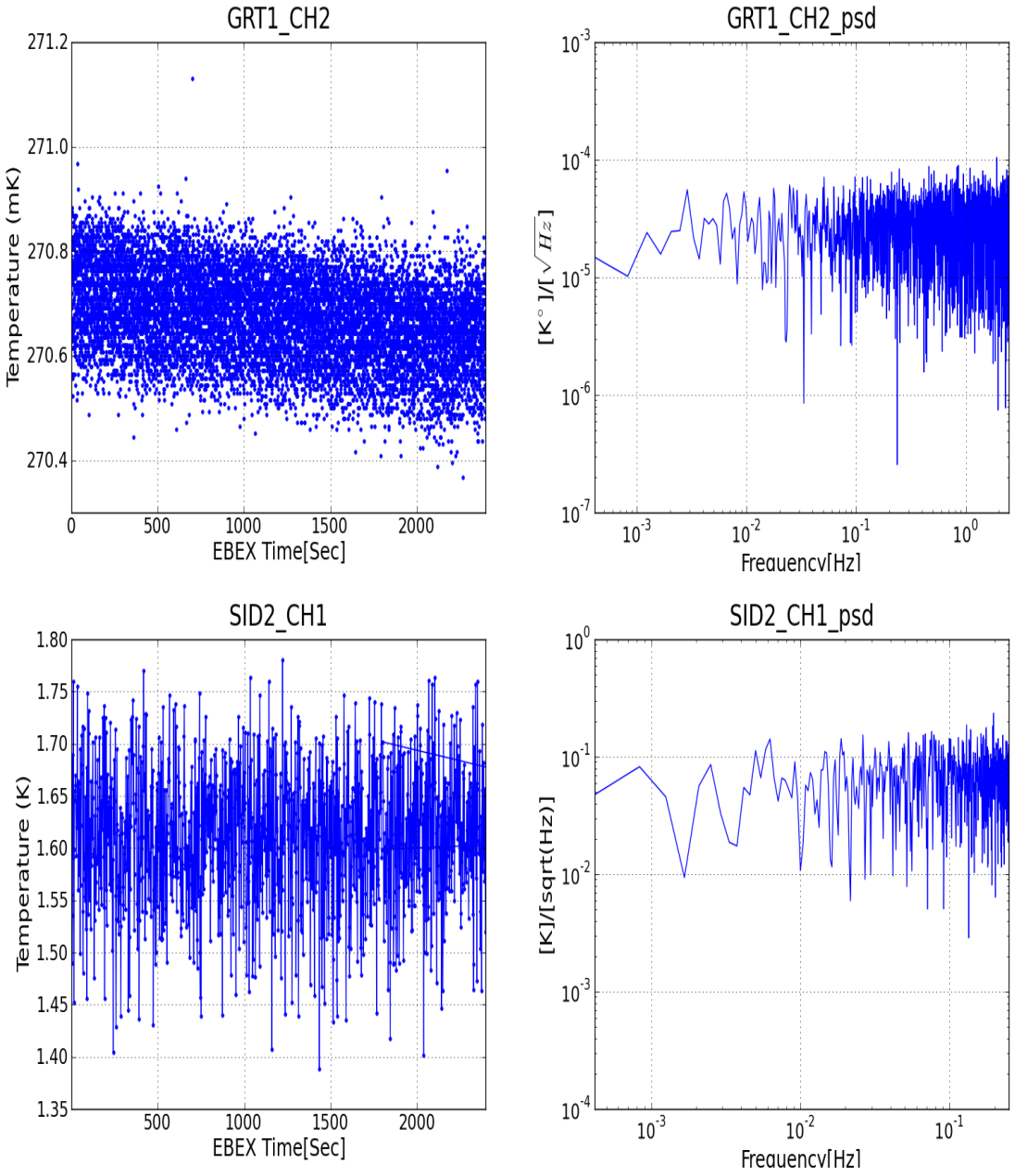

Figure 4.12: Top left: 410 GHz wafer temperature during the wide slew scan. Top right: power spectrum of the temperature data on the left. Bottom left: Optics box temperature during the wide slew scan. Bottom right: power spectrum of the temperature data on the left.

Chapter 5

Disk Pressure Vessels

In the Antarctic science flight EBEX will have 1960 bolometers that are sampled at a rate of 190.73 Hz. Every data sample is 16 bits which gives a total data rate of 0.75 Mbyte/sec. In addition the approximately 100 channels of ACS sampled at 100.16 Hz contribute 20 kbyte/sec. Two HWP channels sampled at 3.03 kHz produce data at a rate of 12 kBytes/sec. These give a combined data rate of 0.78 Mbytes/sec. Two redundant copies of the complete data set are written to disk by the two flight computers, each copy to a physically separate disk array. This adds up to a total of 1.9 Tbytes of data during a 14 day flight.

Standard hard drives are not designed to operate in a vacuum environment. Ensuring correct separation between the read/write head and the magnetic media requires the presence of air. At typical balloon altitudes the pressure is a few Torr, which renders standard hard drives non operational. Therefore, I designed and constructed two sealed pressure vessels which enclose the hard drives and ensure atmospheric pressure throughout the flight.

Solid state disks do not require atmospheric pressure in order to operate. However, due to the large volume of data and the high cost of solid state drives at the time the choice was made, standard 2.5" laptop hard drives [47] are used. Laptop hard drives are designed to survive mishandling and are more robust than standard desktop 3.5" drives.

Each disk is mounted on an Advance Technology Attachment over Ethernet (ATAoE)

interface board[1] [48] making it accessible over Ethernet. The ATAoE communication protocol enables us to have a network topology that allows access to any disk by any computer as illustrated in figure 5.1 which shows the EBEX network design for the long duration flight. The ring topology of the network offers protection against a single point failure; if a connection breaks, the hard drive is still accessible via the other side of the ring.

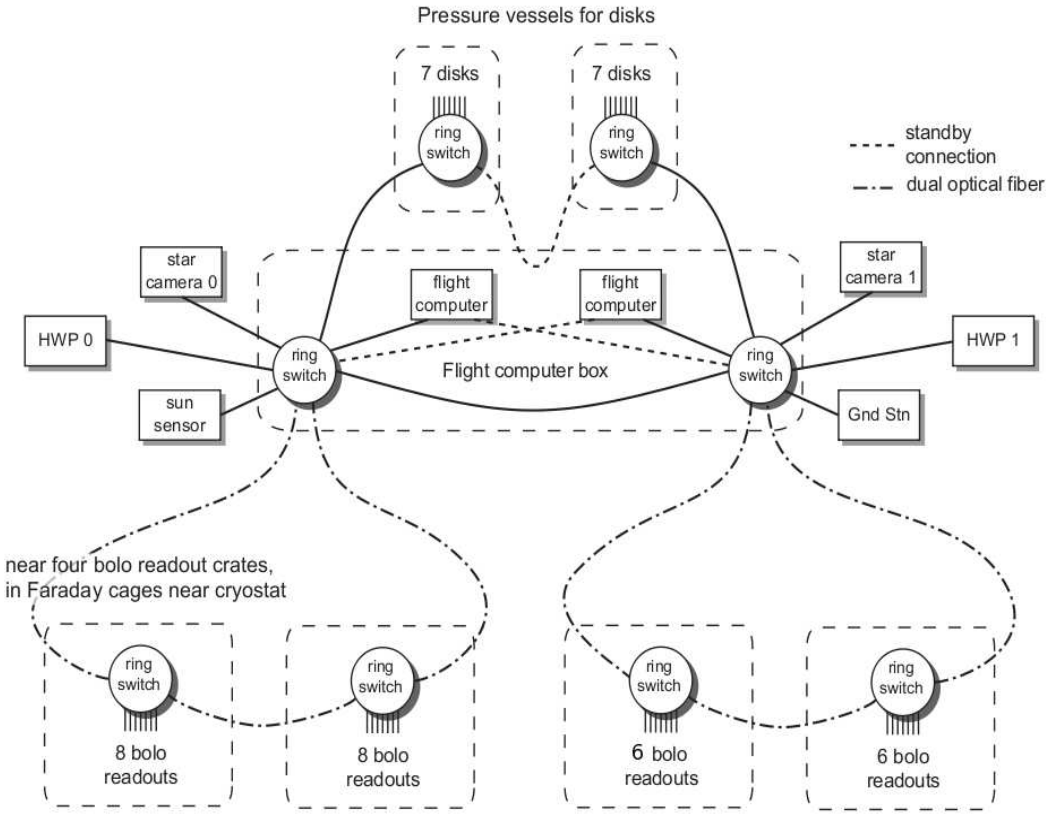

Figure 5.1: EBEX network diagram.

[1] These boards are no longer available as the manufacturer shifted to producing multiple disk arrays accessible over Ethernet rather than single disks.

5.1 Design

The pressure vessel is an aluminum cylinder, 20" long with a diameter of 8" and a wall thickness of 0.125". It is closed with a welded cap on one end and has a flange on the other. The hoop stress σ_θ on the walls of the cylinder is given by [49]: $\sigma_\theta = \frac{P \cdot R}{b}$ where P is the pressure inside the pressure vessel, R is its radius and b is the wall thickness. The result, 3.25 MPa, is more than a factor of ten lower than the Tensile strength of the aluminum. A rectangular inner frame is mounted onto the lid of the pressure vessel. The inner frame includes a backplane circuit board that provides the following:(1) power and network interface for up to eight hard drives; (2) power for two fans that circulate the air inside the pressure vessels and improve heat flow by convection; (3) power for a temperature triggered heater with a set point of -20C to prevent components from freezing; (4) four temperature sensors [44] - two mounted on the circuit board at its edges and two more on the hard drives themselves; and (5) a pressure sensor [50].

A network switch [51] with two ring ports and seven regular ports is mounted on top of the inner frame. To prevent overheating of the network switch's processor the switch was removed from its case and mounted with the processor facing the wall of the cylinder. The lid includes a KF 25 port for pumping the pressure vessel and a hermetic feed-through connector with 37 pins that brings signals and power to and from the flight computer crate. The temperature and pressure sensors are readout by the GHK board (see section 4.2.1) in the flight computer crate. A silicone O-ring was used.

5.1.1 Power consumption

The power consumption of the pressure vessel is listed in table 5.1.

Component	Power [W] each	Power total [W]
Network switch	3	3
Fans	0.5	1
ATAoE blade	1.8	12.6
Idle disk	1.4	7
Writing disk	2.6	5.2
Total power	28.8	

Table 5.1: Pressure vessel power consumption. Each pressure vessel includes one network switch, two fans, seven ATAoE disk blades and assuming five idle disks and two writing disks.

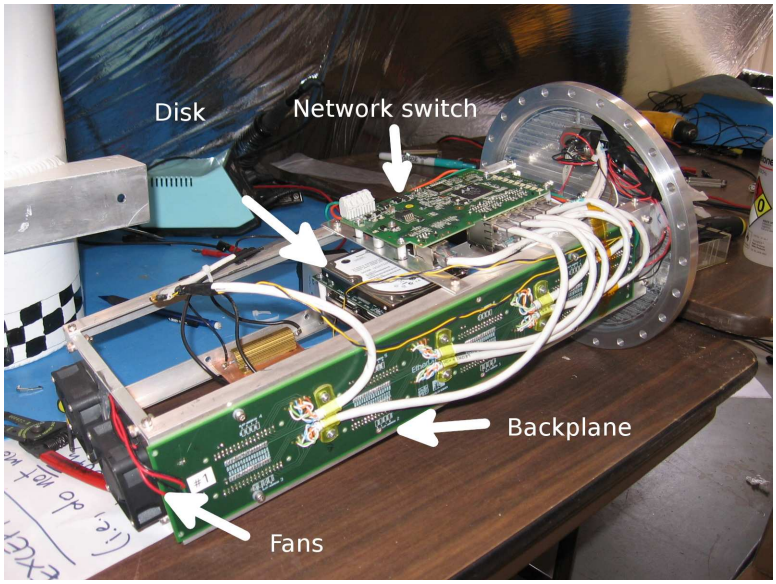

Figure 5.2: A photograph of the pressure vessel inner frame. The backplane is mounted on the near side with Ethernet wires connecting it to the network switch (top). The disk is plugged into the backplane. The fans are mounted on the left hand side of the inner frame.

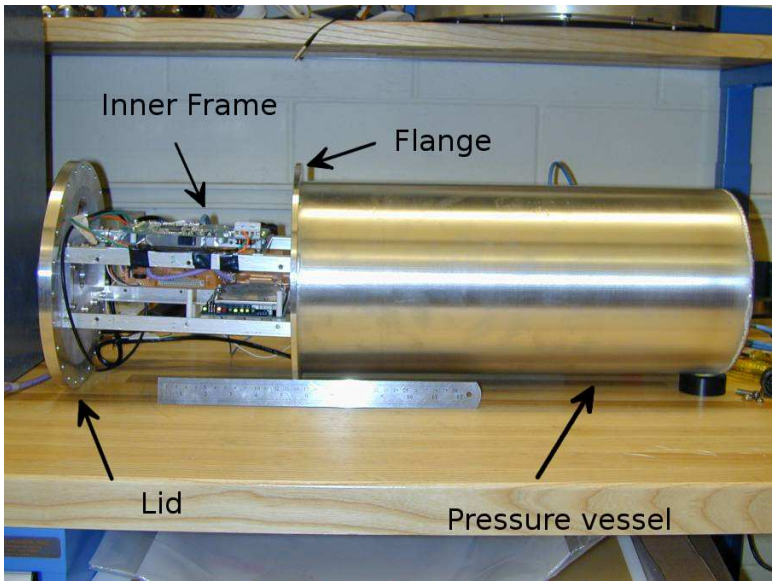

Figure 5.3: A photograph of the pressure vessel shell. The lid with the inner frame attached is extended from the pressure vessel

5.2 Test Flight

Before the test flight the pressure vessels were pumped out (while powered down) then pressurized to 0.85 atmospheres with dry nitrogen gas. This value keeps the pressure near atmospheric when in the temperature range of -30C - +30C. The pressure vessel was then wrapped with a thermal blanket to prevent over-cooling during ascent.

During the pre-flight instrument integration several problems prevented the use of the nominal design configuration (figure 5.1). When two pressure vessels were connected to the flight computer at the same time a firmware version mismatch between the network switches caused the flight computer to crash. This issue was bypassed by using a single pressure vessel during the flight. In addition, the General Housekeeping board in the flight computer crate was not used, due to an unresolved grounding problem. A temperature sensor mounted on the hard drives, originally designated to be read out by the General housekeeping board, was rerouted to be readout as an ACS slow channel.

An additional temperature sensor was mounted on the external shell of the pressure vessel as part of the gondola temperature sensors. The data from these sensors is shown in figure 5.4.

The pressure vessel's positioning on the gondola is such that it is not exposed to the sky but rather hidden behind baffles. The main concern before the flight was that the components would get too cold. Nevertheless, the flight data shows that this was not an issue. During the ascent and passing through the tropopause when the ambient temperature was as low as -55C° the pressure vessel did not get below -13°C.

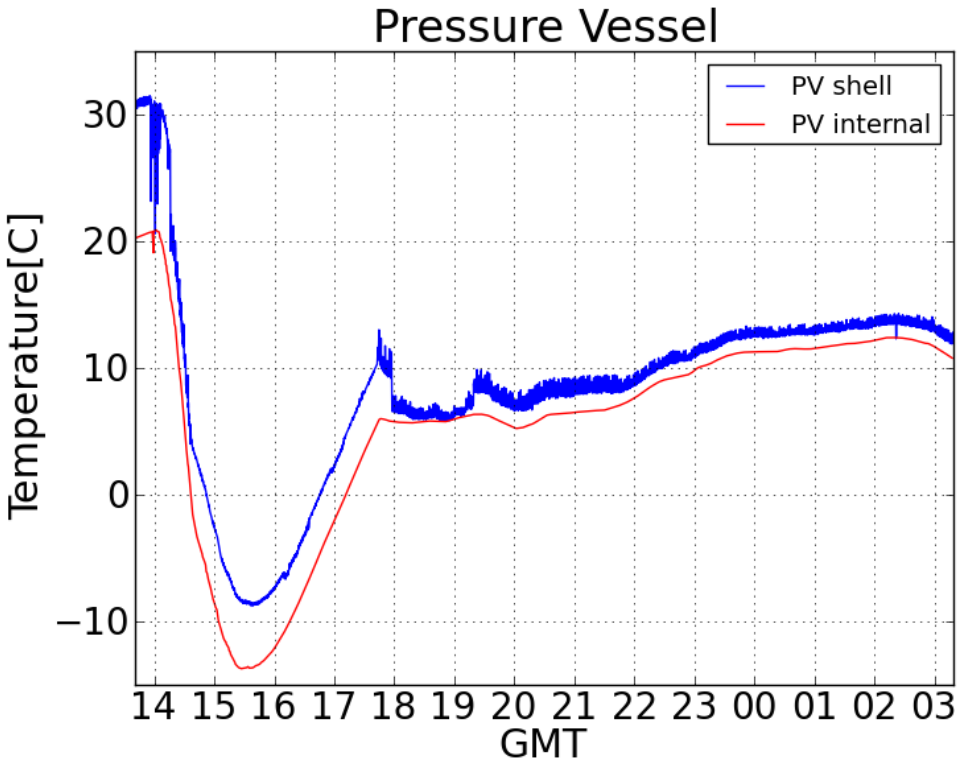

Figure 5.4: The temperature of the disk pressure vessel during the test flight.

During the flight there were no problems with the hard drives. Two copies of the data were written, one by each flight computer, to two different hard drives mounted in the same pressure vessel.

Chapter 6

Cryostat Power and Grounding

EBEX uses more than 1300 Watts of power to operate. This power is used to control the gondola, to operate bolometers and to collect and store data from the bolometers, the pointing and the housekeeping sensors. Two parallel power systems are operated in EBEX: the Attitude Control System (ACS) power, and the Cryostat power domains. The ACS power domain includes the flight computers and all the motors and sensors which are required for pointing the instrument. It is considered a noisey power domain. The cryostat power domain includes the Dfmux boards, the cryostat housekeeping electronics and the Half Wave Plate (HWP) system. To prevent interference from the ACS noise in the bolometer signals these two systems are isolated from each other.

In the test flight each power domain was powered by a separate bank of non rechargeable 28 V batteries. In the Antarctic science flight separate banks of rechargeable batteries to be charged by separate solar panels will be used.

I commissioned and tested the Cryostat power domain, tracking its performance in the lab, during the test flight and in preparation for the Antarctic science flight.

6.1 Cryostat Power Domain

The cryostat power domain includes the following subsystems: Bolometer power, Network power, Housekeeping power, Heater power and HWP power. Power from the batteries is routed in parallel to two bolometer power crates mounted on each side of the gondola. DC/DC converters are used to convert voltage from the 28 V batteries

to the voltage required by each subsystem. The DC/DC converters are high efficiency converters with an operating temperature range between -55°C to +125°C [52].

Power crate 1 includes DC/DC converters for all the subsystems in the Cryostat power domain. Bolometer power is routed from power crate 1 to Bolometer Readout (BRO) crates 1 and 3. The HWP system receives direct 28 V battery power which goes through a relay in power crate 1. Power crate 2 includes DC/DC converters only for Bolometer power which is routed to BRO crate 2 and 4.

Typically DC/DC converters have a voltage sense feature to compensate for the voltage drop along the lines between the converter and the load. In EBEX, powering two different readout crates from a single power crate requires that the sense line be attached to the output bus at the power crate. Any compensation for voltage drop in the lines is done by tuning up the output voltage.

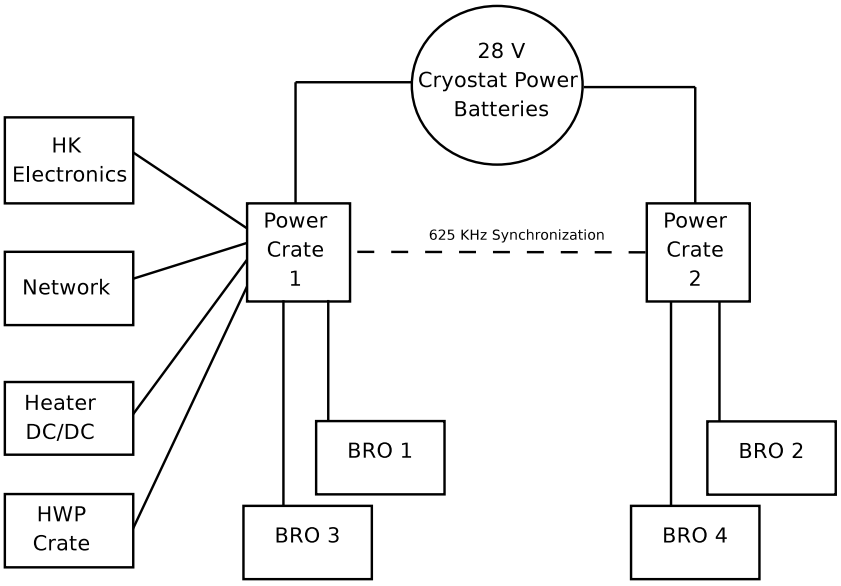

Figure 6.1: A schematic diagram of the EBEX cryostat power domain.

Figure 6.1 shows a schematic representation of the Cryostat power domain. The main consumers of power in the Cryostat power domain are the Dfmux boards. The boards require ±6 V for their operation. Each board uses approximately 20 W, 80% of which is drawn from +6 V. Three 120 W converters [53] are used in parallel to supply

the +6 V voltage and a single DC/DC converter is used supply -6 V. Two [54] DC/DC converters are used to supply ±10 V which is routed via the Dfmux boards to the SQUID controller boards. Table 6.1 shows the total power from each voltage. The values in the table are measured values for the test flight and calculated values for the science flight. The values include the DC/DC converter efficiency of 82%. The Heater power is only used during a refrigerator cycle. The HWP power is given for a steady state rotation at 2 Hz.

Name	Voltage[V]	Power[W] (NA)	Power[W] (LDB)
Bolometer	$\pm 6\,V, \pm 10\,V$	298	695
Net	$+12\,V$	21	38
Heater	$+13\,V, +26\,V$	3.5	
Housekeeping	$+5.8\,V, -9.6\,V$	12	
HWP	$+28\,V$	42	
Total		376.5	790.5

Table 6.1: Power used in the cryostat power domain during the test flight (NA) and the Antarctic science flight (LDB).

Thermal Performance

The efficiency of the converters was measured to be 82%. The converters are attached thermally to a 0.25" aluminum base plate of the power crate so that heat dissipated in the converter is conducted away and radiated to the sky. During the test flight a temperature sensor mounted on the base plate reached a maximum temperature of 13.2 C°. The power crate temperature during the test flight is shown in figure 6.2.

Control

A separate CSBF[1] discrete science stack signal (SIP) is used to control the state of a solid state relay [55] which controls the input power to each subsystem's DC/DC. The SIP signal received via the ACS system is kept isolated from the cryostat power domain.

[1] Columbia Scientific Ballooning Facility

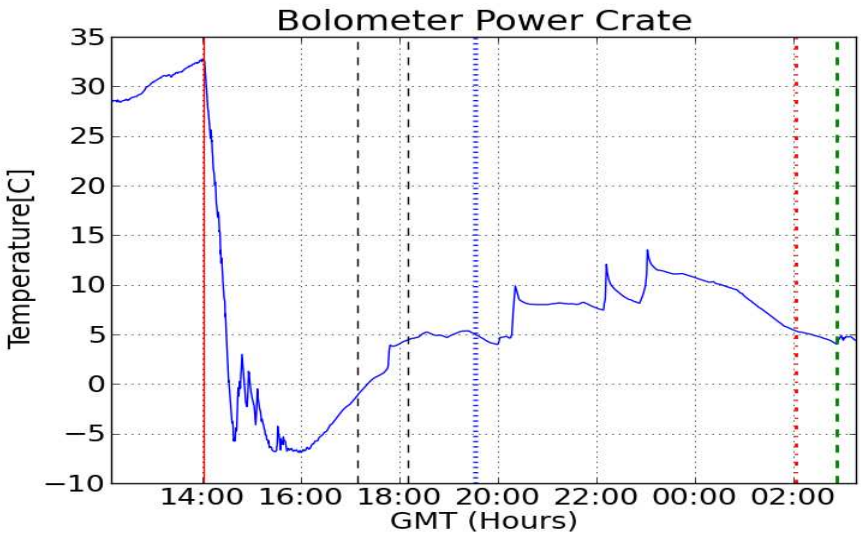

Figure 6.2: Temperature of the base plate of Power crate 1 during the test flight. The spikes between 20:00 and 23:00 GMT correspond to the gondola pointing in the direction of the sun.

In addition to the system level control allowed by the SIP, a higher resolution of control is given by digital I/O commands issued over the CANbus. The network, heater and bolometer DC/DC converters in each power crate can be inhibited separately, using the General housekeeping board. Each BRO can be powered off using the McGill clock board which is commanded by the time server board. In addition, each HWP subsystem (DC motor, laser diode, gripper motors) has a designated solid state relay that is controlled by digital I/O signals from the General housekeeping board.

Switching Frequency

The switching frequency of the DC/DC converters is externally synchronized to a 625 kHz signal which is produced by an oscillator board in the power crates. Power crate 1 contains the master board which includes the oscillator. Power crate 2 contains only a slave board. The slave board receives the synchronization signal from the master board and distributes it to the DC/DC converters in the power crate.

During the test flight the switching frequency synchronization was found to increase

the noise levels in the bolometers and SQUIDS. Therefore, it was disabled. When not synchronized to an external signal, the switching frequency of the DC/DC converters ranges from 525 kHz - 625 kHz.

6.2 Grounding

A ground loop occurs when there is more than one path connecting a part of the system to the system ground, which is the reference electrical potential. The duplicate ground paths form the equivalent of a loop antenna which picks up interference efficiently. This will cause voltage fluctuations in the leads. As a consequence of these voltage fluctuations, the ground reference in the system is no longer a stable potential. This can cause increased noise and systematic errors in the data.

As part of the general effort to reduce systematic effects in EBEX, special care was taken in designing the grounding scheme. The two main design guidelines were: (a) to separate and to isolate the signal shields[2] from the current return lines, and (b) to ground each subsystems to a central star ground by only one point.

This was not the case for the bolometer system. There, the connector back-shells and board ground are at the same potential. As a result when a board is plugged into its crate, the ground of the board (power return) and the crate are shorted to each other via the front panel screws of the board. Since BRO crates were mounted directly to the gondola, special care was taken to isolate the chassis of the BRO from its mounting bracket. The cryostat body and the BRO were electrically connected to each other.

Special care was taken to keep the cryostat power system isolated from the ACS power system. Lines which span both systems such as the Ethernet network, the CAN-bus and the time bus, had their signals transferred over optics fiber between the two power domains. The cryostat is electrically isolated from the gondola by using G10 spacers. It is connected to the star ground, located at the bottom of the gondola, by a grounding strap. Before the test flight this electrical isolation was confirmed before connecting the cryostat to the star ground. Figure 6.3 shows the electrical connection in the cryostat power domain. The power return of NET power, HK power and BOLO power are connected using ferrites.

[2] A metallic layer creating a Faraday cage around a cable or connector

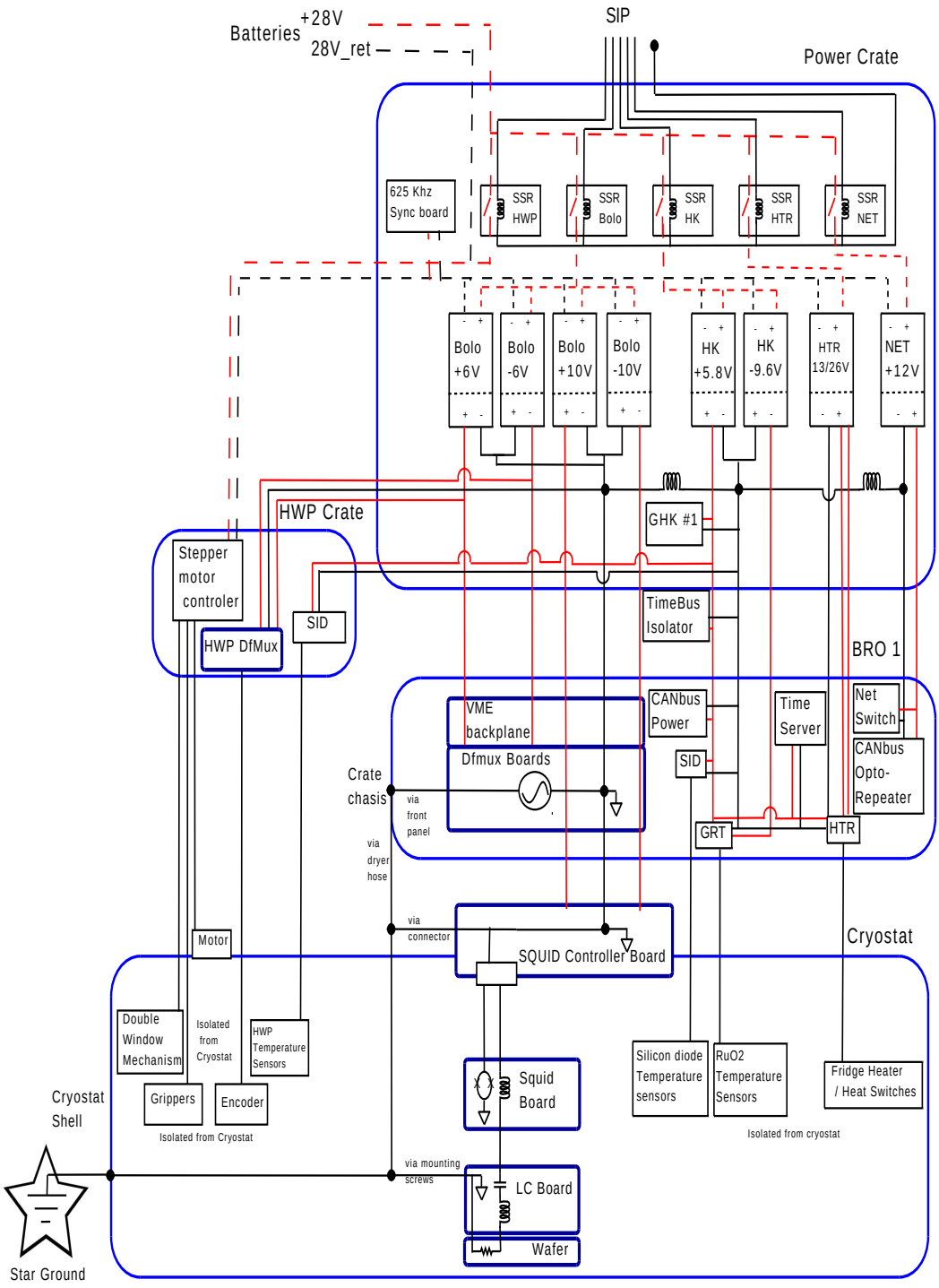

Figure 6.3: Power and ground connections in the Cryostat power domain. Dashed lines represent raw battery power; Solid lines represent electrical connections; Red lines represent power lines; Signals into the cryostat are represented by a single line; Dark blue squares represent the BOLO power domain.

Chapter 7

Calibrator Flashes

Responsivity of a bolometric detector depends on the physical properties of the detector, on the optical load incident on the detector, and on the temperature of the bath to which the detector is thermally linked. In order to calibrate any variation in responsivity during the flight and between subsequent system tune-ups, an internal calibrator is used. I developed the hardware and software required to flash the calibrator and assessed its performance during the test flight.

7.1 Hardware

Two light emitting diodes (LED)[56] were installed at the edge of each of the three bolometer wafer holders used in the test flight. Figure 7.1 shows a model drawing of a wafer, its holder and its circuit board to which the LED were mounted. All six LED were connected in parallel to a single pair of wires that was routed via the RF tower (see section 2.5.5) and the cryostat housekeeping wiring to a heater board channel (see section 4.2.4). A bias resistor at the output of the heater board was used to set the current to the LED to 10 μA.

A script running on a ground station computer sent a command to flash the LED, twice every 15 minutes. The command was sent to the flight computer via telemetry. Once received at the flight computer, this command triggered a sequence of CANbus messages sent to the heater board, which would turn on the LED channel, wait 250 μsec and then turn it off. After a 250 μsec pause the process was repeated. Each command

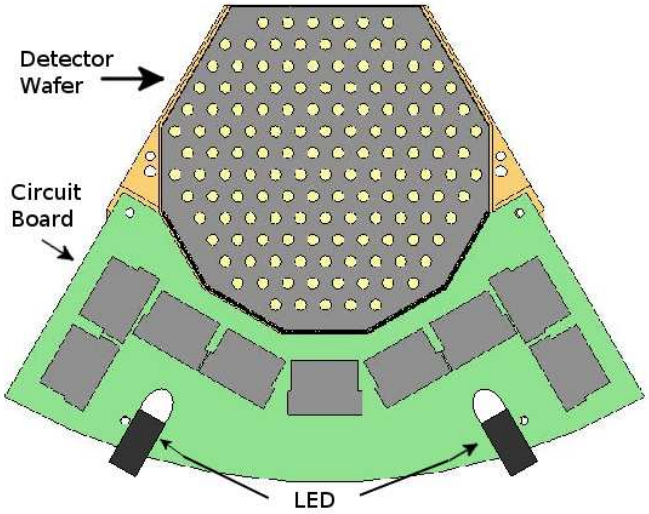

Figure 7.1: Illustration of an EBEX detector wafer with two LED mounted on it.

to turn the LED on or off required a sequence of two CANbus messages.

The flight computer code consumed approximately 2% of the available CPU cycles. Under these conditions, kernel scheduling granularity, which is set to 4 msec, is the dominant uncertainty in the length of programmed delays. Any programmed delay of less than 4 msec will end up being at least 4 msec, or two to three times that value. Therefore, the LED flash was longer than what was specified in the code, and the LED was turned on for an average of $\sim$12 msec.

In addition to variations in the waiting time by the flight computer, the delay between sending the CANbus messages by the flight computer and the heater board carrying out the commands depends on the CANbus traffic load and may vary between subsequent commands. These variations may be on the order of one millisecond [57].

7.2 Calibrating Responsivity Change

A review of infrared bolometers is given in [58]. The EBEX detectors are described in several publications [18][59].

In this section an estimation for the requirements from a calibrator used in EBEX

is given. For a constant voltage biased transition edge sensor (TES), as used in EBEX, the current responsivity is given by:

$$S_I = \frac{\Delta I}{\Delta P_{op}} = \frac{-1}{V_b} \cdot \frac{\mathcal{L}}{\mathcal{L}+1} \tag{7.1}$$

where V_b is the voltage bias of the TES and $\mathcal{L}$ is the TES electro-thermal feedback loop-gain. The loop-gain characterizes the strength of the electro-thermal feedback and is given by[1] :

$$\mathcal{L} = \frac{P_e \alpha}{GT} \tag{7.2}$$

Where P_e is the electrical power biasing the detector, T is the temperature of the detector, G is the average thermal conductance of the detector's weak link to the bath and $\alpha \equiv \frac{d(log(R))}{d(log(T))}$. The responsivity of a few EBEX detectors was measured before the test flight to range from $10^5 - 10^6 \frac{Amp}{W}$[60].

7.2.1 Bath Temperature Dependence

The dependence of responsivity on bath temperature (T_0) is found by:

$$\frac{dS_I}{dT_0} = \frac{dS_I}{d\mathcal{L}} \frac{d\mathcal{L}}{dP_{el}} \frac{dP_{el}}{dT_0} = \frac{1}{V_b} \frac{1}{(\mathcal{L}+1)^2} \frac{\kappa(T_0)}{\kappa(T)} \cdot \frac{1}{T} \cdot \alpha \tag{7.3}$$

where κ is the thermal conductivity of the bolometer's weak link to the bath. To find the relative change in the responsivity we look at:

$$\frac{\Delta S}{S} = \frac{\frac{dS}{dT_0} \cdot \Delta T_0}{S} = \frac{1}{\mathcal{L}(\mathcal{L}+1)} \frac{\kappa(T_0)}{\kappa(T)} \cdot \alpha \frac{\Delta T_0}{T} \tag{7.4}$$

The values of V_b, $\mathcal{L}$ and α are challenging to measure and may vary between detectors. To get an order of magnitude estimate for how responsivity will be affected by a change in bath temperature we use the assumption that $\kappa(T) = \kappa_0 \cdot T^n$, with n=2. Figure 7.2 shows resistance vs. temperature data from a TES bolometer in a test cryostat measured by Kate Raach. From the plot we measure $\alpha \approx 2800$. The voltage bias for this detector was $\sim V_b = 3\mu$V. Taking an approximate value for G=60 pW/K, we calculate from equation 7.2 $\mathcal{L} \approx 1000$ (T=T_c=413.5 mK, T_0=320 mK, R=1.2 Ω).

[1] This is the zero frequency loop-gain

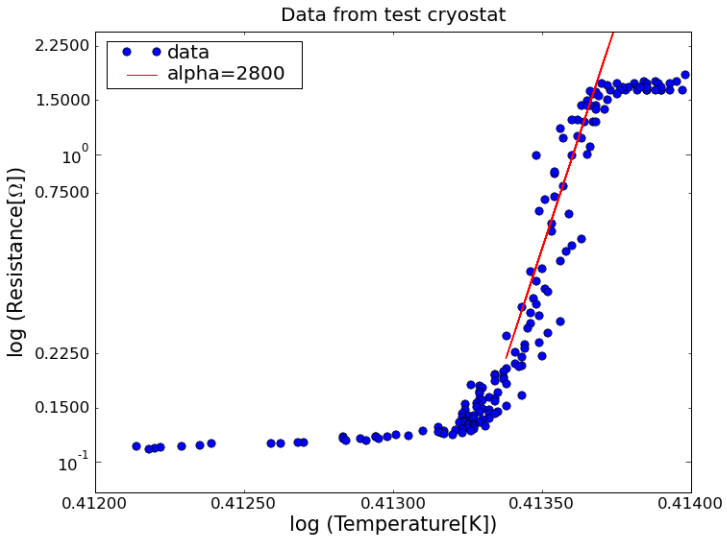

Figure 7.2: Resistance vs. temperature data of a TES bolometer

This gives:

$$\frac{\Delta S}{S} = 3 \cdot 10^{-3} \cdot \frac{\Delta T_0}{T} \tag{7.5}$$

So for every change of 1% in the bath temperature the responsivity will change by 0.003%. Even if we take a factor of ten safety margin for the approximation done here, there is still a ratio of 1 to 30 in the affect bath temperature has on the bolometer responsivity. The change in responsivity is suppressed by the loop-gain squared but is enhanced by α.

Actual temperature drift

During the test flight a ruthenium dioxide temperature sensor was mounted on each of the wafers. Figure 7.3 shows the data from these sensors between 19:30 UTC and the end of the flight. Once the focal plane's temperature stabilized after being warmed during the bolometer system tune-up, the temperature remained stable to within 2 mK for the remainder of the flight. This temperature variation is less than 0.8% of the wafer temperature. This variation in temperature causes a variation of less than 0.01%

in responsivity, which is negligible. In order to calibrate such changes in responsivity the calibrator signal would have to be stable to at least a 0.01% level.

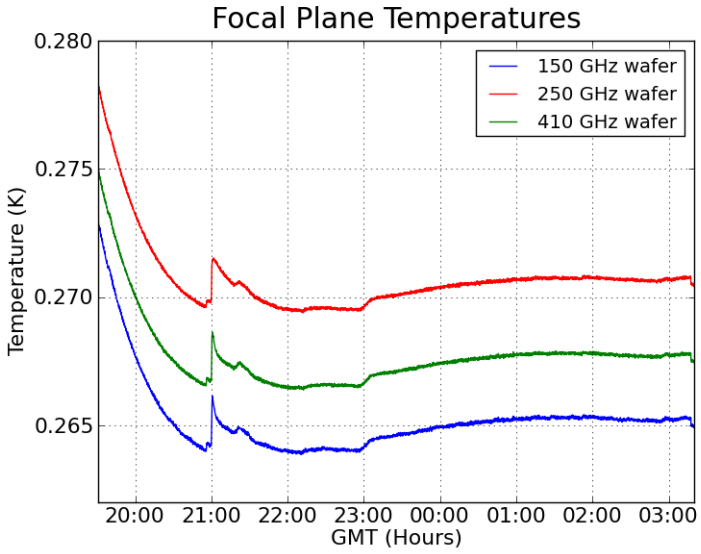

Figure 7.3: Temperature data of the wafer RuO_2 temperature sensors during the test flight

7.2.2 DC Optical Loading

When a higher DC optical load is incident on the TES, less electrical power is required to keep the TES biased in its transition. This affects the detector's dynamic range and also its responsivity. The dependence of responsivity on the DC level of incident optical power is found by:

$$\frac{dS_I}{dP_{dc}} = \frac{dS_I}{d\mathcal{L}} \frac{d\mathcal{L}}{dP_{el}} \frac{dP_{el}}{dP_{op}}$$

Which gives:

$$\frac{dS_I}{dP_{dc}} = \frac{-1}{V_b} \frac{\mathcal{L}}{(1+\mathcal{L})^2} \frac{1}{P_{el}} \tag{7.6}$$

To find the relative change we look at:

$$\frac{\Delta S}{S} = \frac{(\frac{dS}{dP_{dc}}) \cdot \Delta P_{dc}}{S} = \frac{1}{(\mathcal{L}+1)} \frac{\Delta P_{dc}}{P_{el}} \tag{7.7}$$

Using the same values as in section 7.2.1 we get:

$$\frac{\Delta S}{S} = 1.3 \cdot 10^{-4} \cdot \Delta P_{dc}\ [pW] \tag{7.8}$$

Variations in the DC power incident on the detectors can be caused by several factors such as the CMB dipole or the galactic plane. These factors are sub dominant to the affect of atmospheric loading. At the floating altitude of the balloon the instrument is above most of the atmosphere. Nevertheless, when the elevation angle of the telescope changes with respect to the Earth's horizon, the loading from the atmosphere will change. The change will depend on the altitude of the balloon and on the elevation angle of the telescope. The extent of these effects is summarized in Figure 7.4 [61].

To estimate how these effects will change the bolometer responsivity we take a value of ΔP_{DC}= 20 pW, which will cause a 0.26% change in responsivity. As with bath temperature, the stability of the calibrator must be at least better than what it is used to calibrate.

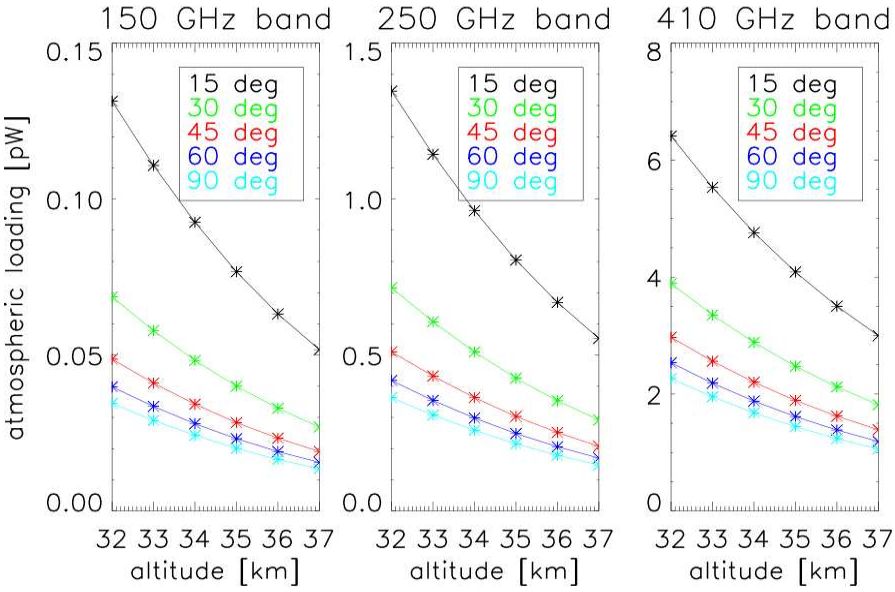

Figure 7.4: Optical loading at the EBEX frequency bands as a function of altitude. Data is given for an elevation of 15°, 30°, 45°, 60° and 90°. The plot was created by Chaoyun Bao.

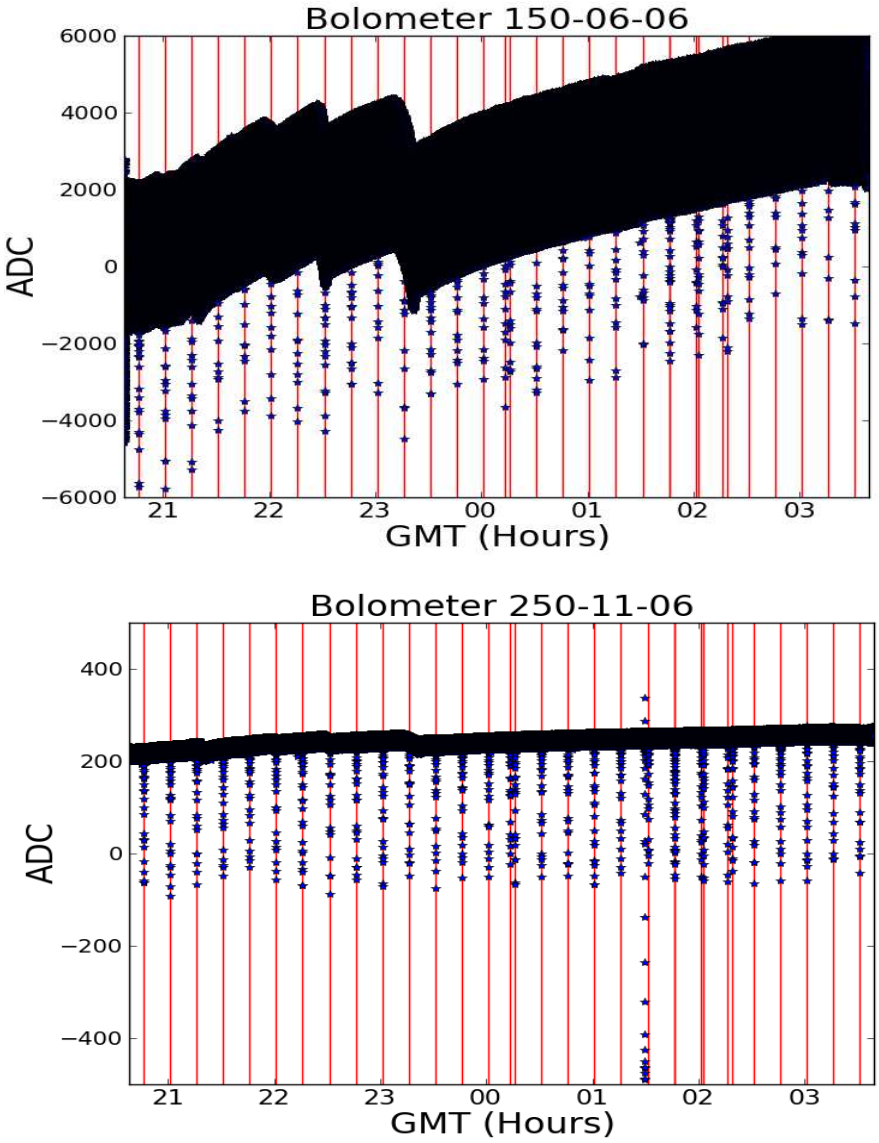

Figure 7.5: Unprocessed data from a bolometer on the 150 GHz wafer (top) and the 250 GHz wafer (bottom). The red lines represent the times at which a calibrator flash command was received on the flight computer

7.3 Test Flight Flashes

An analysis was performed on data from the LED flashes to find out whether the configuration of the LED during the test flight was suitable as an internal calibrator.

The bolometers and SQUIDs were tuned during the test flight. At approximately 20:15 GMT the tuning was completed. At 20:26 GMT the first calibrator flash command was received at the flight computer. Figure 7.5 shows the data from one bolometer on the 150 GHz wafer and one bolometer on the 250 GHz wafer during the period after the bolometers were tuned until the end of the flight at 03:30 AM.

The bolometer data is dominated by the signal from rotation of the HWP (see figure 7.6). In order to compare the amplitudes of the LED signals at different times regardless of the orientation of the HWP, thirty seconds of data preceding the flash were fit to a 12 harmonic template that was then subtracted from the flash data along with an offset and a slope. The residual of this process is the signal from calibrator flash alone. Figure 7.6 shows a calibrator flash before and after the HWP template removal. After the HWP template was removed from the flashes, they can be compared.

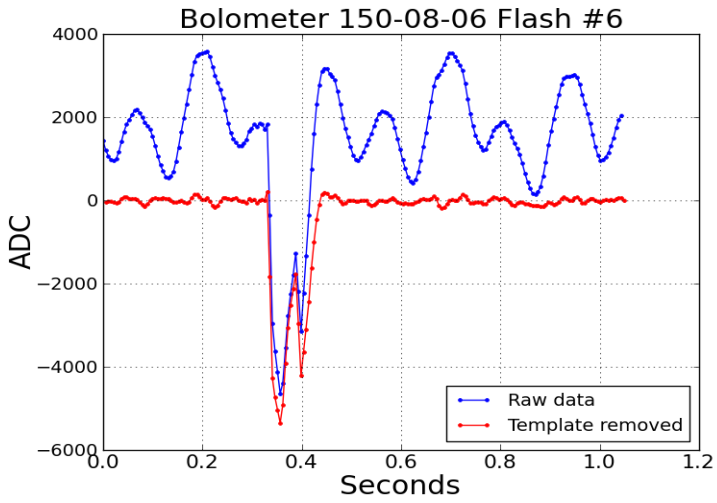

Figure 7.6: A single event of unprocessed calibrator flash data (blue) and after removing the HWP template (red).

The focal plane during the test flight included 202 detectors that were distributed into three groups: 167 detectors open to light, 22 dark dark detectors used for systematic checks, and 13 eccosorb-horn filled bolometers that had ∼99% of the light attenuated for calibration measurements before the flight. However, the position of the LED on the circuit board had the light pass between the horn array and the wafer. Therefore there is no distinguishing between the three types of bolometers with regard to the LED flash signal. Figures 7.7, 7.8 and 7.9 show a single flash event from each group for each wafer. No flash signal was measured for the 410 GHz dark detectors. The distance between the LED and a detector can be inferred from the detector name: (wafer)-(row)-(column). A low row value is closer to to the LED (see figure 7.1).

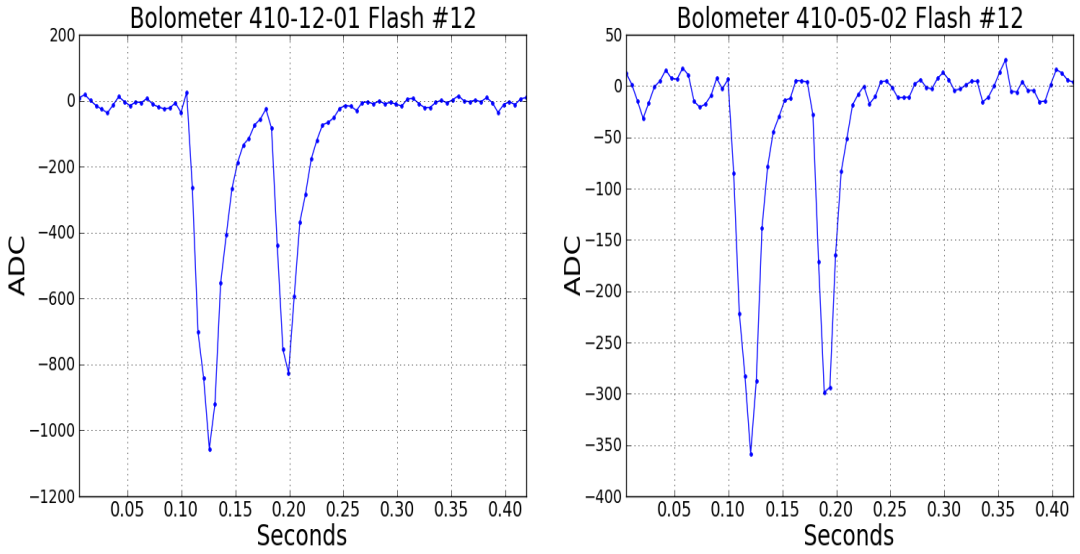

Figure 7.7: 410 GHz wafer LED flashes from a detector open to light (left) and with an eccosorb plug (right).

Figure 7.10 shows the peak value of the flash signals for a 250 GHz bolometer for all LED flashes during the test flight. The spread of the peak values in this plot is 70 counts, which are approximately 20% of the peak value. This spread is actually one of the more consistent detectors. For some detectors the spread in flash value was more than 100% of the peak value.

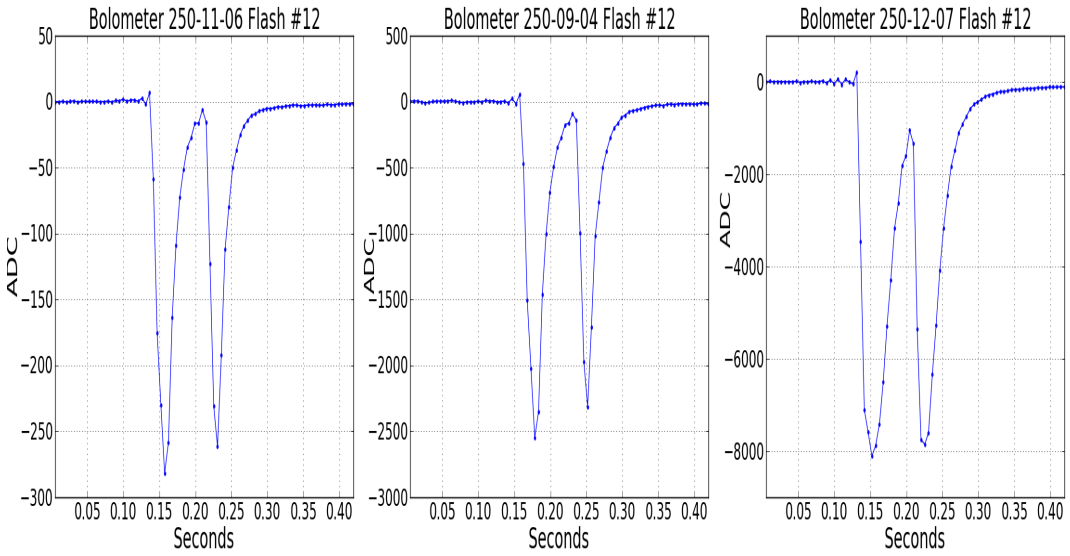

Figure 7.8: 250 GHz wafer LED flashes from a detector open to light (left) an eccosorb plugged detector (middle) and a dark detector (right).

As noted above the temperature of the wafer was stable during this period so temperature variation is ruled out as the cause for the large spread in LED flash peak signal value.

The large spread of the peak values of the LED flash signal renders it useless as a calibrator.

Why didn't it work / Discussion

For a single flash, the LED was on for approximately 12 msec. This time is similar to the bolometer time constant ($\approx$ 15 msec). For the bolometer to reach a steady state (96%) the optical signal should be on for at least three time constants. If the LED is on for less than this, then the bolometer does not yet reach a steady state, and the amplitude of its signal depends on how long the signal was integrated on.

As mentioned in section 7.1 the time that the LED was on was not constant nor repeatable. The combination of a short flash with an irregular flash length caused the

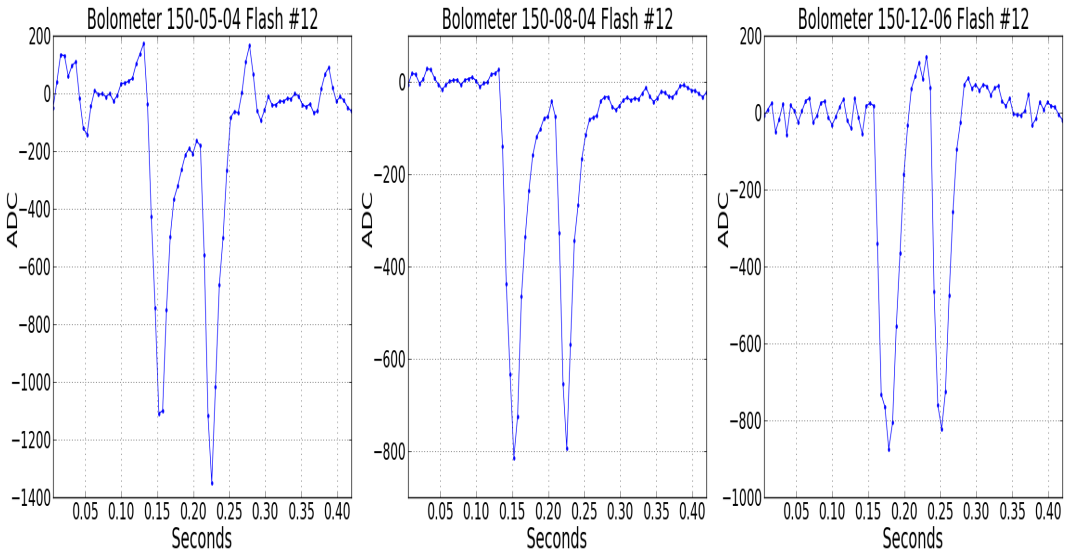

Figure 7.9: 150 GHz wafer LED flashes from a detector open to light (left) an eccosorb plugged detector (middle) and a dark detector (right).

various flashes to be at random amplitudes, and not adequate to calibrate the responsivity.

7.4 Future plans

The data from the test flight shows that the LED configuration was not suitable as a calibrator. For the long duration science flight the LED will be replaced by a stimulator. The stimulator consists of a thin nickel-chromium 2 mm x 2 mm square that is backed by a sapphire substrate. The metal layer is impedance matched to radiate efficiently into free space when heated. It was successfully used in Maxima [62] as an internal calibrator.

The stimulator will be mounted inside the optics box opposite the grid, so that its signal can be detected by both focal planes. The stimulator will be powered by a heater board channel.

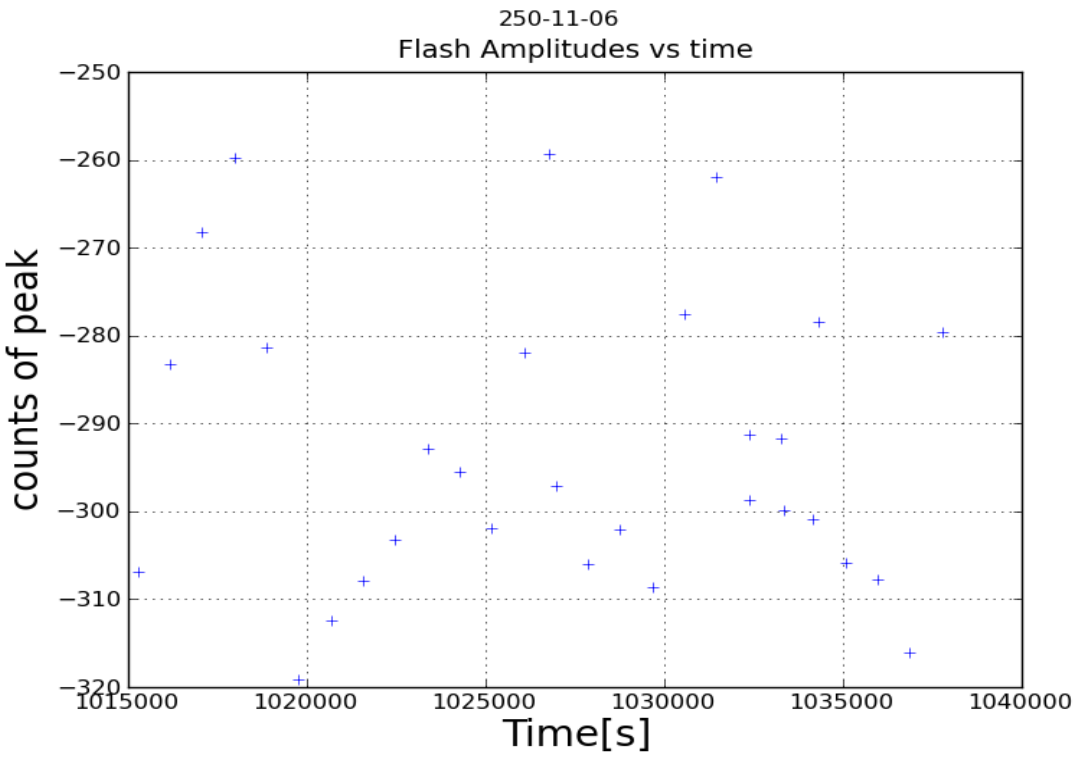

Figure 7.10: The magnitude of all the calibrator flash signal for a single 250 GHz bolometer during the test flight.

References

[1] H. Reeves. Cosmological Turtles. *Nuclear Physics B Proceedings Supplements*, 80:9–11, March 2000.

[2] R. H. Dicke, P. J. E. Peebles, P. G. Roll, and D. T. Wilkinson. Cosmic Black-Body Radiation. *Ap. J.* , 142:414–419, July 1965.

[3] E. Komatsu, K. M. Smith, J. Dunkley, C. L. Bennett, B. Gold, G. Hinshaw, N. Jarosik, D. Larson, M. R. Nolta, L. Page, D. N. Spergel, M. Halpern, R. S. Hill, A. Kogut, M. Limon, S. S. Meyer, N. Odegard, G. S. Tucker, J. L. Weiland, E. Wollack, and E. L. Wright. Seven-year Wilkinson Microwave Anisotropy Probe (WMAP) Observations: Cosmological Interpretation. *Ap. J. Suppl.* , 192:18–+, February 2011, 1001.4538.

[4] D. Baumann, M. G. Jackson, P. Adshead, A. Amblard, A. Ashoorioon, N. Bartolo, R. Bean, M. Beltrán, F. de Bernardis, S. Bird, X. Chen, D. J. H. Chung, L. Colombo, A. Cooray, P. Creminelli, S. Dodelson, J. Dunkley, C. Dvorkin, R. Easther, F. Finelli, R. Flauger, M. P. Hertzberg, K. Jones-Smith, S. Kachru, K. Kadota, J. Khoury, W. H. Kinney, E. Komatsu, L. M. Krauss, J. Lesgourgues, A. Liddle, M. Liguori, E. Lim, A. Linde, S. Matarrese, H. Mathur, L. McAllister, A. Melchiorri, A. Nicolis, L. Pagano, H. V. Peiris, M. Peloso, L. Pogosian, E. Pierpaoli, A. Riotto, U. Seljak, L. Senatore, S. Shandera, E. Silverstein, T. Smith, P. Vaudrevange, L. Verde, B. Wandelt, D. Wands, S. Watson, M. Wyman, A. Yadav, W. Valkenburg, and M. Zaldarriaga. Probing Inflation with CMB Polarization. In S. Dodelson, D. Baumann, A. Cooray, J. Dunkley, A. Fraisse, M. G. Jackson, A. Kogut, L. Krauss, M. Zaldarriaga, & K. Smith , editor, *American Institute of*

Physics Conference Series, volume 1141 of *American Institute of Physics Conference Series*, pages 10–120, June 2009, 0811.3919.

[5] A. Linde. Inflationary Cosmology. In *Inflationary Cosmology*, volume 738 of *Lecture Notes in Physics, Berlin Springer Verlag*, pages 1–+, 2008, 0705.0164.

[6] J. C. Mather, E. S. Cheng, D. A. Cottingham, R. E. Eplee, D. J. Fixsen, T. Hewagama, R. B. Isaacman, K. A. Jensen, S. S. Meyer, P. D. Noerdlinger, S. M. Read, L. P. Rosen, R. A. Shafer, E. L. Wright, C. L. Bennett, N. W. Boggess, M. G. Hauser, T. Kelsall, S. H. Moseley, R. F. Silverberg, G. F. Smoot, R. Weiss, and D. T. Wilkinson. Measurement of the cosmic microwave background spectrum by the COBE FIRAS instrument. *Ap. J.* , 420:439–444, January 1994.

[7] G. F. Smoot, C. L. Bennet, A. Kogut, E. L. Wright, J. Aymon, N. W. Boggess, E. S. Cheng, G. De Amici, S. Gulkis, M. G. Hauser, G. Hinshaw, P. D. Jackson, M. Janssen, E. Kaita, T. Kelsall, P. Keegstra, C. Lineweaver, K. Lowenstein, P. Lubin, J. Mather, S. S. Meyer, S. H. Moseley, T. Murdock, L. Rokke, R. F. Silverberg, L. Tenorio, R. Weiss, and D. T. Wilkinson. Structure in the COBE Differential Microwave Radiometer First-Year Maps. *Ap. J.* , 396:L1–L5, 1992.

[8] D. Larson, J. Dunkley, G. Hinshaw, E. Komatsu, M. R. Nolta, C. L. Bennett, B. Gold, M. Halpern, R. S. Hill, N. Jarosik, A. Kogut, M. Limon, S. S. Meyer, N. Odegard, L. Page, K. M. Smith, D. N. Spergel, G. S. Tucker, J. L. Weiland, E. Wollack, and E. L. Wright. Seven-year Wilkinson Microwave Anisotropy Probe (WMAP) Observations: Power Spectra and WMAP-derived Parameters. *Ap. J. Suppl.* , 192:16–+, February 2011, 1001.4635.

[9] W. Hu and M. White. A CMB polarization primer. *New Astronomy*, 2:323–344, 1997. astro-ph/9706147.

[10] U. Seljak and M. Zaldarriaga. Signature of Gravity Waves in the Polarization of the Microwave Background. *Phys. Rev. Lett.* , 78:2054–2057, March 1997. astro-ph/9609169.

[11] H. C. Chiang, P. A. R. Ade, D. Barkats, J. O. Battle, E. M. Bierman, J. J. Bock, C. D. Dowell, L. Duband, E. F. Hivon, W. L. Holzapfel, V. V. Hristov, W. C.

Jones, B. G. Keating, J. M. Kovac, C. L. Kuo, A. E. Lange, E. M. Leitch, P. V. Mason, T. Matsumura, H. T. Nguyen, N. Ponthieu, C. Pryke, S. Richter, G. Rocha, C. Sheehy, Y. D. Takahashi, J. E. Tolan, and K. W. Yoon. Measurement of Cosmic Microwave Background Polarization Power Spectra from Two Years of BICEP Data. *Ap. J.* , 711:1123–1140, March 2010, 0906.1181.

[12] B. Gold, N. Odegard, J. L. Weiland, R. S. Hill, A. Kogut, C. L. Bennett, G. Hinshaw, X. Chen, J. Dunkley, M. Halpern, N. Jarosik, E. Komatsu, D. Larson, M. Limon, S. S. Meyer, M. R. Nolta, L. Page, K. M. Smith, D. N. Spergel, G. S. Tucker, E. Wollack, and E. L. Wright. Seven-year Wilkinson Microwave Anisotropy Probe (WMAP) Observations: Galactic Foreground Emission. *Ap. J. Suppl.* , 192:15–+, February 2011, 1001.4555.

[13] F. Stivoli, C. Baccigalupi, D. Maino, and R. Stompor. Separating polarized cosmological and galactic emissions for cosmic microwave background B-mode polarization experiments. *MNRAS* , 372:615–629, October 2006, astro-ph/0505381.

[14] U. Seljak. Measuring Polarization in the Cosmic Microwave Background. *Ap. J.* , 482:6–16, June 1997. astro-ph/9608131.

[15] M. Zaldarriaga and U. Seljak. Gravitational lensing effect on cosmic microwave background polarization. *Physics Review D.* , 58:23003 (6 pages), July 1998.

[16] W. N. Brandt, C. R. Lawrence, A. C. S. Readhead, J. N. Pakianathan, and T. M. Fiola. Separation of foreground radiation from cosmic microwave background using multifrequency measurements. *Ap. J.* , 424:1, 1994.

[17] C. Baccigalupi. Cosmic microwave background polarisation: foreground contrast and component separation. *New Astronomy Review*, 47:1127–1134, December 2003.

[18] J. Hubmayr, F. Aubin, E. Bissonnette, M. Dobbs, S. Hanany, A. T. Lee, K. MacDermid, X. Meng, I. Sagiv, and G. Smecher. Design and characterization of TES bolometers and SQUID readout electronics for a balloon-borne application. In *SPIE Conference Series*, volume 7020, August 2008.

[19] M. D. P. Truch, P. A. R. Ade, J. J. Bock, E. L. Chapin, J. Chung, M. J. Devlin, S. Dicker, M. Griffin, J. O. Gundersen, M. Halpern, P. C. Hargrave, D. H. Hughes,

J. Klein, C. J. MacTavish, G. Marsden, P. G. Martin, T. G. Martin, P. Mauskopf, C. B. Netterfield, L. Olmi, E. Pascale, G. Patanchon, M. Rex, D. Scott, C. Semisch, N. E. Thomas, C. Tucker, G. S. Tucker, M. P. Viero, and D. V. Wiebe. The Balloon-borne Large Aperture Submillimeter Telescope: BLAST. In *American Astronomical Society Meeting Abstracts #213*, volume 41 of *Bulletin of the American Astronomical Society*, pages 475.04–+, January 2009.

[20] B. Reichborn-Kjennerud. *Building and Flying the E and B Experiment to Measure the Polarization of the Cosmic Microwave Background*. PhD thesis, Columbia University, 2010.

[21] Precision Cryogenic Systems Inc., Indianapolis, IN.

[22] P. A. R. Ade, G. Pisano, C. Tucker, and S. Weaver. A review of metal mesh filters. In *Society of Photo-Optical Instrumentation Engineers (SPIE) Conference Series*, volume 6275 of *Presented at the Society of Photo-Optical Instrumentation Engineers (SPIE) Conference*, July 2006.

[23] S. Hanany, H. Hubmayr, B. R. Johnson, T. Matsumura, P. Oxley, and Thibodeau M. Millimeter-wave achromatic half-wave plate. *Applied Optics*, 44:4666–4670, August 2005.

[24] T. Matsumura, S. Hanany, P. Ade, B. R. Johnson, T. J. Jones, P. Jonnalagadda, and G. Savini. Performance of three- and five-stack achromatic half-wave plates at millimeter wavelengths. *Applied Optics*, 48(19):3614–3625, June 2009.

[25] S. Hanany, T. Matsumura, B. Johnson, T. Jones, J. R. Hull, and K. B. Ma. A cosmic microwave background radiation polarimeter using superconducting bearings. *IEEE Transactions on Applied Superconductivity*, 13:2128–2133, June 2003.

[26] J Klein. et al. Cryogenic Half-Wave Plate Polarimeter Using a Superconducting Magnetic Bearing. *In preparation*, 2011.

[27] M. E. Huber, P. A. Neil, R. G. Benson, D. A. Burns, A. M. Corey, C. S. Flynn, Y. Kitaygorodskaya, O. Massihzadeh, J. M. Martinis, and G. C. Hilton. DC SQUID Series Array Amplifiers with 120 MHz Bandwidth. *IEEE Transactions on Applied Superconductivity*, page 1251, March 2001.

[28] M. Dobbs, E. Bissonnette, and H. Spieler. Digital Frequency Domain Multiplexer for Millimeter-Wavelength Telescopes. *IEEE Transactions on Nuclear Science*, 55:21–26, 2008, 0708.2762.

[29] Tekdata Interconnections Limited, UK.

[30] Chase Research Cryogenics ltd.

[31] Parker Hannifin, rectangular strip EMI gasket.

[32] Spectrum Control, part numbers: 56-735-004.

[33] Amphenol FPT02 Series; 60-db Attenuation at 1.0 GHz.

[34] M. Zaldarriaga and S. Leach. Effects of Pointing Errors. *Internal project memo*, 2006.

[35] Valpey-Fisher, model: VFTDR-EC20V5S-10.00 MHz.

[36] W. Stallings. In *Data and Computer Communications (7th ed.)*, pages 137–138. Prentice Hall, 2004. ISBN: 0-13-100681-9.

[37] C. Plummer, P. Roos, and L. Stagnaro. CAN Bus as a Spacecraft Onboard Bus. In *DASIA 2003*, volume 532 of *ESA Special Publication*, 2003.

[38] The ATLAS Collaboration. The ATLAS Experiment at the CERN Large Hadron Collider. *Journal of Instrumentation*, 3:8003–+, August 2008.

[39] B. Hallgren, H. Boterenbrood, H. J. Burckhart, and H. Kvedalen. The embedded local monitor board (ELMB) in the LHC front-end I/O control. 7th Workshop Electron. LHC Experiments, Stockholm, Sweden, 2000.

[40] CANopen application layer and communication profile, cia draft standard 301, version 4.02, 13 february 2002 http://www.can-cia.de.

[41] Kvaser, leaf semi-pro.

[42] Adfweb - Industrial Electronic Devices, Optic fibers repeaters for CANbus, HD67117F.

[43] Analog Devices, AD7661: 16-bit, 100 ksps pulsar unipolar ADC with ref.

[44] Analog Devices,AD590: 2-terminal IC temperature transducer.

[45] Lakeshore Cryotronics Inc. Westerville, OH.

[46] Lakeshore, Ruthenium oxide temperature sensor 102-A.

[47] Seagate,2.5" Momentus 5400 rpm.

[48] Coraid, 2.5" ATA-over-Ethernet blade controller.

[49] D. Roylance. Pressure Vessels. *Department of Materials Science and Engineering, Massachusetts Institute of Technology*, August 2001.

[50] Freescale Semiconductor, Integrated pressure sensor, MPX4115A.

[51] Sixnet, SLX-9RS-ST.

[52] Crane Aerospace and Electronics, Interpoint brand.

[53] http://www.interpoint.com/products/product_listing/mor/.

[54] http://www.interpoint.com/products/product_listing/mhv/.

[55] Crydom, part number: D1D40.

[56] Fairchild Semiconductor, IR LED, LED56.

[57] J. Kaiser and M. A. Livani. Invocation of Real-Time Objects in a CAN Bus System. In *I st lnt 7 Symposium on Object-Oriented Distributed Real-Time Computing Systems*, 1998.

[58] P. L. Richards. Bolometers for infrared and millimeter waves. *Journal of Applied Physics*, 76:1–24, July 1994.

[59] F. Aubin, A. M. Aboobaker, P. Ade, C. Baccigalupi, C. Bao, J. Borrill, C. Cantalupo, D. Chapman, J. Didier, M. Dobbs, W. Grainger, S. Hanany, J. Hubmayr, P. Hyland, S. Hillbrand, A. Jaffe, B. Johnson, T. Jones, T. Kisner, J. Klein, A. Korotkov, S. Leach, A. Lee, M. Limon, K. MacDermid, T. Matsumura, X. Meng,

A. Miller, M. Milligan, D. Polsgrove, N. Ponthieu, K. Raach, B. Reichborn-Kjennerud, I. Sagiv, G. Smecher, H. Tran, G. S. Tucker, Y. Vinokurov, A. Yadav, M. Zaldarriaga, and K. Zilic. First implementation of TES bolometer arrays with SQUID-based multiplexed readout on a balloon-borne platform. In *Society of Photo-Optical Instrumentation Engineers (SPIE) Conference Series*, volume 7741 of *Presented at the Society of Photo-Optical Instrumentation Engineers (SPIE) Conference*, July 2010.

[60] J. Hubmayr. Ground Based Measurement of Bolometer Responsivity. Internal EBEX project memo, 2009.

[61] C. Bao. Atmospheric Loading Calculation for EBEX NA Flight. Internal EBEX project memo, 2011.

[62] B. Rabii. *MAXIMA: Observations of CMB anisotropy.* PhD thesis, University of California, Berkeley, 2002.